

Atlantic Multidecadal Oscillation and Northern Hemisphere's climate variability

Marcia Glaze Wyatt · Sergey Kravtsov ·
Anastasios A. Tsonis

Received: 31 August 2010 / Accepted: 4 April 2011 / Published online: 13 April 2011
© Springer-Verlag 2011

Abstract Proxy and instrumental records reflect a quasi-cyclic 50–80-year climate signal across the Northern Hemisphere, with particular presence in the North Atlantic. Modeling studies rationalize this variability in terms of intrinsic dynamics of the Atlantic Meridional Overturning Circulation influencing distribution of sea-surface-temperature anomalies in the Atlantic Ocean; hence the name Atlantic Multidecadal Oscillation (AMO). By analyzing a lagged covariance structure of a network of climate indices, this study details the AMO-signal propagation throughout the Northern Hemisphere via a sequence of atmospheric and lagged oceanic teleconnections, which the authors term the “stadium wave”. Initial changes in the North Atlantic temperature anomaly associated with AMO culminate in an oppositely signed hemispheric signal about 30 years later. Furthermore, shorter-term, interannual-to-interdecadal climate variability alters character according to polarity of the stadium-wave-induced prevailing hemispheric climate regime. Ongoing research suggests mutual interaction between shorter-term variability and the stadium wave, with indication of ensuing modifications of multidecadal variability within the Atlantic sector. Results presented here support the hypothesis that AMO plays a significant role in hemispheric and, by inference, global climate variability,

with implications for climate-change attribution and prediction.

Keywords Climate indices · Teleconnections · AMO · NAO · ENSO · PDO

1 Introduction

A pressing challenge for climate science in the era of global warming is to better distinguish between climate signals that are anthropogenically forced and those that are naturally occurring at decadal and longer timescales. Identifying the latter is essential for assessing relative contributions of each component to overall climate variability.

Multi-century proxy records reflect the signature of such a low-frequency climate signal, paced at a typical timescale of 50–80 years, with pronounced presence in the North Atlantic (Stocker and Mysak 1992; Mann et al. 1995; Black et al. 1999, Shabalova and Weber 1999; Delworth and Mann 2000; Gray et al. 2004). A similar signature has been detected in the instrumental record (Folland et al. 1986; Kushnir 1994; Schlesinger and Ramankutty 1994; Mann and Park 1994, 1996; Enfield and Mestas-Nuñez 1999; Delworth and Mann 2000; Zhen-Shan and Xian 2007). Modeling studies, with divergent results dependent upon model design (Delworth et al. 2007; Msadek et al. 2010a), qualitatively support this pattern and tempo of variability in terms of the Atlantic Meridional Overturning Circulation's (AMOC) influencing redistribution of sea-surface-temperature (SST) anomalies in the Atlantic Ocean (Delworth and Mann 2000; Dong and Sutton 2002; Latif et al. 2004; Knight et al. 2005). Observed multidecadal SST variability in the North Atlantic Ocean, believed

M. G. Wyatt (✉)
Department of Geologic Sciences, CIRES, Benson
Earth Sciences Building, University of Colorado-Boulder,
Boulder, CO 80309, USA
e-mail: marciaw Wyatt@earthlink.net

S. Kravtsov · A. A. Tsonis
Department of Mathematical Sciences, Atmospheric Sciences
Group, University of Wisconsin-Milwaukee,
Milwaukee, WI 53201-0413, USA

consequent of variability in the AMOC, has been termed the Atlantic Multidecadal Oscillation (AMO: Kerr 2000; Enfield et al. 2001).

AMO significantly impacts climate in North America and Europe (Enfield et al. 2001, Sutton and Hodson 2005, Knight et al. 2006; Pohlmann et al. 2006). In fact, its influence may have a global character; a suite of studies have addressed bits and pieces of requisite interactions (Dong and Sutton 2002, 2007; Dima and Lohmann 2007; Grosfeld et al. 2008; Sutton and Hodson 2003, 2005, 2007; Sutton et al. 2003; Timmermann et al. 2007; Zhang and Delworth 2005, 2007; Zhang et al. 2007; Polyakov et al. 2009).

Atlantic-related multidecadal variability reflected in geographically diverse proxy and instrumental records, combined with an abundance of numerical studies that link the hemispheric climate signal to AMO-related North Atlantic variability, guide our hypothesis and motivate our present investigation. We endeavor to put these previous results into perspective through use of a statistical methodology that characterizes Northern Hemispheric multidecadal climate variability and provides rigorous statistical bounds on the associated uncertainties. Emergent is a picture of a climate signal propagating from the North Atlantic throughout the Northern Hemisphere via a sequence of atmospheric and lagged oceanic teleconnections. We term this signal the “stadium wave”. The stadium wave is examined here both in terms of its role in generating a multidecadally varying hemispheric climate signature and in its relationship with interannual-to-interdecadal climate variability.

Our philosophical approach, data sets, and analysis methods are described in Sect. 2. Section 3 contains the results of our analyses. Section 4 summarizes our work and discusses potential mechanisms underlying the stadium wave.

2 Approach, data sets and methods

2.1 Approach

Our strategy was to evaluate collective behavior within a network of climate indices. Considering index networks rather than raw 3-D climatic fields is a relatively novel approach that has its own advantages—such as potentially increased dynamical interpretability, along with apparent increase of signal-to-noise ratio, and enhanced statistical significance—at the expense of detailed phenomenological completeness. In particular, the climate indices may represent distinct subsets of dynamical processes—tentatively, “climate oscillators”—that might, however, exhibit various degrees of coupling (Tsonis et al. 2007). As these

indices also pertain to different geographical regions, we directly address the question of the global multidecadal teleconnections. Using fairly standard multivariate statistical tools, we aim to characterize dominant mode of climate co-variability in the Northern Hemisphere and provide rigorous estimates of its statistical significance, namely: What are the chances that the low-frequency alignment of various regional climatic time series, alluded to in an impressive suite of previous climate studies (see Sect. 1), is, in fact, random? Our methodology allows us to give a quantitative answer to this question. Furthermore, objective filtering of the multidecadal signal provides a clearer picture of higher-frequency climate variability and its possible multi-scale interactions within the climate system.

2.2 Data sets

Insights gained from extensive literature review regarding proxy records, instrumental data, and climate-model studies; completeness of data sets throughout the twentieth century; and preliminary examination of linearly detrended 30-year smoothed index-anomaly time series (not shown), collectively prompted our choice to use two subsets of climate indices to address our hypotheses. A main set of eight indices focused on the role played by the stadium-wave teleconnection sequence in the evolution of the multidecadal hemispheric climate signal. Seven complementary indices were then used to generate a larger fifteen-member network (Table 1);¹ the goals here were to (1) check the robustness of our results to the choice of index subset; (2) to paint a more complete picture of multidecadal variability; and (3) to investigate more fully the role of higher-frequency behavior in relation to multidecadal stadium-wave propagation.

The original subset of eight indices contained the Northern Hemisphere area-averaged surface temperature (NHT), the Atlantic Multidecadal Oscillation (AMO), Atmospheric-Mass Transfer anomaly (AT), the North Atlantic Oscillation (NAO), El Niño/Southern Oscillation (NINO3.4), the North Pacific Oscillation (NPO), the Pacific Decadal Oscillation (PDO), and the Aleutian Low Pressure (ALPI) indices. The complementary set of seven indices used to generate our expanded network included: the North Pacific Gyre Oscillation (NPGO), ocean-heat-content anomalies of the upper 700 and 300 meters in the North Pacific Ocean (OHC700 and OHC300), the Pacific North American (PNA) pattern, the Western Pacific (WP) pattern, the Pacific Meridional Mode (PMM), and the Atlantic

¹ The time series of the indices used is later shown in Fig. 7, in terms of their decomposition into multidecadal signal and remaining higher-frequency variability.

Table 1 Observed climate-index network

Index/acronym	Reference/data source	Description/general information
Aleutian Low Pressure Index AL or ALPI	Beamish et al. (1997) http://www.pac.dfo-mpo.gc.ca/sci/sa-mfpd/downloads/indices/alpi.txt	Relative intensity of SLP in N. Pacific (~50°N) in winter (DJFM) Calculated as mean area (km ²) w/SLP < 100.5 kPa. Expressed as anomaly relative to the 1950–1997 mean
Atlantic Multidecadal Oscillation Index AMO	Kerr (2000), Enfield et al. (2001), and Sutton and Hodson (2003) http://www.esrl.noaa.gov/psd/data/timeseries/AMO/	North Atlantic SSTA averaged across 0–60°N, 75–7.5°W; 1871–2003 Monopolar SSTA pattern N. Atlantic
Atlantic Meridional Mode Index AMM	Chiang and Vimont (2004) http://www.cdc.noaa.gov/Timeseries/Monthly/AMM/ http://www.aos.wisc.edu/~dvimont/Research/MModes/Data/AMM.txt	SST projected onto 10-m wind field 21°S–32°N; 74°W–15°E; SST gradient across intertropical convergence zone (ITCZ) in Atlantic. (proxy for position of Atlantic ITCZ) (Observations available from 1949)
Atmospheric-Mass Transfer Anomalies AT	Vangenheim (1940) and Girs (1971) http://www.alexeyiyubushin.narod.ru/lyubushin@yandex.ru	Dominance of air transfer direction 30°–80°N; 45–75°E; proxy for atmospheric-heat transfer; reflects longitudinal/latitudinal shifts in position of atmospheric centers-of-action, w/implications for hemispheric communication of climate signal
North Atlantic Oscillation Index NAO	Hurrell (1995) http://www.cgd.ucar.edu/cas/jhurrell/indices.data.html#npanom	Normalized SLP difference Azores and Iceland ~ 1st PC (principal component) of SLP in the North Atlantic; re-distribution of atmospheric mass b/n subpolar and subtropical latitudes, reflecting jet-stream variations
Northern Hemisphere Temperature NHT	Jones and Moberg (2003) and Rayner et al. (2006) ftp://ftp.cru.uea.ac.uk/data http://www.cru.uea.ac.uk/cru/data/temperature/hadcrut3nh.txt	Average surface land and sea-surface temperatures of Northern Hemisphere 1850–2003 NHT characterizes overall climate variability, with strongest changes occurring at high northern latitudes
El Niño/Southern Oscillation Region 3.4 NINO3.4	Calculated from the HadSST1 http://www.cdc.noaa.gov/gcos_wgsp/Timeseries/Data/nino34.long.data	Average SSTA 5°N–5°S; 170°W–120°W
North Pacific Gyre Oscillation Index NPGO	Di Lorenzo et al. (2008) http://www.o3d.org/npgo/data/NPGO.txt http://www.eros.eas.gatech.edu/npgo/	Proxy for ENSO behavior 2-nd PC of SSH in NE Pacific. Measures changes in North Pacific gyre circulation (Observations available since 1950)
North Pacific Oscillation Index NPO	Rogers (1981), Walker and Bliss (1932), and Wang et al. (2007) http://www.wangjin@mail.iap.ac.cn http://www.wangjin@mail.iap.ac.cn	Meridional dipole in SLP over North Pacific; pressure variations b/n Hawaii and Alaska/Alberta, reflective of meridional re-distribution of atmospheric mass. We used that of Wang et al. (2007); 2nd EOF SLPA 100°E–120°W, 0°–90°N
Indices of Ocean-Heat-Content Anomalies OHCA300 OHCA700	Willis et al. (2004) http://www.jwillis@pacific.jpl.nasa.gov http://www.nodc.noaa.gov/OC5/DATA_ANALYSIS/basin_data.html	Measured in North Pacific for 0–300 m & 0–700 m upper layers May serve as proxies for ocean-dynamic-induced SST variations (since these are presumably not confined to the oceanic mixed layer, while those caused by atmosphere–ocean heat flux are) (Observations available since 1955)

Table 1 continued

Index/acronym	Reference/data source	Description/general information
Pacific Decadal Oscillation Index	Mantua et al. (1997) and Minobe (1997, 1999) ftp://ftp.atmos.washington.edu/mantua/pnw_impacts/INDICES/PDO.latest	Leading PC of SSTA north of 20°N in North Pacific, with century-scale globally averaged SSTA removed; strongly related to intensity and location of Aleutian Low
PDO		
Pacific Meridional Mode Index	Chiang and Vimont (2004) http://www.cdc.noaa.gov/Timeseries/Monthly/PMM	Anomalous meridional SST gradient across the intertropical convergence zone (ITCZ) in the Pacific; proxy for Pacific ITCZ position; MCA of SST and 10-m winds 32°N–21°S, 175°E–95°W
PMM	http://www.aos.wisc.edu/~dvimont/Research/MModes/Data/PMM.txt	(Observations available since 1949)
Pacific North American Pattern Index	Wallace and Gutzler (1981), Bell and Halpert (1995), and Overland et al. (1999) http://www.jisao.washington.edu/data/pna/	Time series related to combination of standardized 500-hPa geopotential height values (Z) in four centers (Wallace and Gutzler 1981); upper tropospheric pattern associated with PDO; associated with intensity variations and longitudinal shifts of the Aleutian Low and with strength and eastward extent of the East Asian jet.
PNA	http://www.epc.ncep.noaa.gov/products/precip/CWlink/pna/norm.pna.monthly.b5001.current.ascii	$\text{PNA} = 0.25 \times [Z(20^\circ\text{N}, 160^\circ\text{W}) - Z(45^\circ\text{N}, 165^\circ\text{W}) + Z(55^\circ\text{N}, 115^\circ\text{W}) - Z(30^\circ\text{N}, 85^\circ\text{W})]$ (Observations available since 1951)
West Pacific Pattern Index	Wallace and Gutzler (1981) http://www.beringclimate.noaa.gov/data/	Difference in the normalized 500-hPa height anomalies between two points (60°N, 155°E and 30°N, 155°E); upper tropospheric pattern associated with NPO.
WP		Involves latitudinal shifts of AL, with resulting influence on oceanic-gyre frontal boundary and western-boundary dynamics—a potential “hotspot” of oceanic-atmospheric coupling (Sugimoto and Hanawa 2009) (Observations available since 1950)

Meridional Mode (AMM) indices. In order to maintain consistency with previous studies to which we compare our results, some of the analyses below will also include another ENSO index, the NINO3 index based on the Kaplan et al. (1998) sea-surface temperature data set. All of these indices have been used extensively in previous studies and highlight distinctive subsets of climatic processes; see Table 1 for references and brief description of each index.

We focused on boreal winter—the period when seasonally sequestered SST anomalies re-emerge (Alexander and Deser 1995), thereby enhancing conditions for potential oceanic–atmospheric coupling. Allied with this goal, the majority of our indices represent the months DJFM. Exceptions include AMO, AT, and OHC, which are annual; this due to logistics of data acquisition, with expectation of minimal impact on results.

Gapless time series of all eight primary indices over the twentieth century period (1900–1999) are available.² Records are less extensive for the complementary set of seven indices—available for only the second half of the twentieth century. To in-fill missing values, we used a covariance-based iterative procedure (Schneider 2001; Beckers and Rixen 2003; Kondrashov and Ghil 2006) described in Sect. 2.3.2. This procedure assumes co-variability-statistics between continuous and gapped indices remain uniform throughout the century. Therefore, some detected relationships among reconstructed indices in the first half of the twentieth century may partially reflect statistical co-dependencies of late twentieth century indices. We guard against interpreting such relationships in dynamical ways (see Sect. 3.2). Prior to analysis, all raw indices were linearly detrended and normalized to unit variance.

2.3 Methodology

2.3.1 Spatiotemporal filtering and climate-signal identification

Compact description of dominant variability implicit in the multi-valued index time series described in Sect. 2.3 was accomplished by disentangling the lagged covariance structure of this data set via Multichannel Singular Spectrum Analysis (M-SSA; Broomhead and King 1986; Elsner and Tsonis 1996; Ghil et al. 2002). M-SSA is a generalization of the more widely used Empirical Orthogonal Function (EOF; Preisendorfer 1988) analysis. M-SSA excels over EOF analysis in its ability to detect lagged relationships characteristic of propagating signals and has been used extensively to examine various climatic time

series (Vautard and Ghil 1989; Ghil and Vautard 1991; Vautard et al. 1992; Moron et al. 1998; Ghil et al. 2002 and references therein).

M-SSA is, in fact, EOF analysis applied to an extended time series, generated from the original time series, augmented by M lagged (shifted) copies thereof. In M-SSA terminology, each of the multivalued index time series (e.g., AMO, NAO, etc.) is referred to as a channel. Because each multivalued index time series represents a spatial region, eigenfunctions of this extended lagged covariance matrix provide spatiotemporal filters, which define modes that optimally describe lagged co-variability of the original multivariate data set—analogue to EOFs optimally describing zero-lag co-variability.

M-SSA modes are represented in the original index space by their reconstructed components (RC). Each RC is effectively the narrow-band filtered version of an original multivariate time series, whose filters are related to coefficients (EOF weights) of M-SSA decomposition of the time series under consideration. In contrast to principal components (PCs) of EOF analysis, RCs are not mutually orthogonal, but their sum across all M-SSA modes is identical to the original time series. We identify leading M-SSA modes with our climate signal and use the sum of their RCs to visualize variability associated with this climate signal.

2.3.2 Treatment of missing data

As mentioned in Sect. 2.2, records are complete for the eight indices in the original subset, yet are limited for the seven indices comprised in our complementary set—these are available only since about 1950. M-SSA can be used to infill incomplete data sets; hence, we applied this technique to our extended set of 15 climate indices. The imputation procedure was developed in Beckers and Rixen (2003) and Kondrashov and Ghil (2006); it is a simpler version of the method proposed by Schneider (2001). At the initial stage, missing values of each index were replaced by this index's time mean, which was computed over available data points. Anomalies associated with this stage's "climatology" were formed, followed by application of M-SSA to the resulting anomaly field. Time series in channels with missing data were then reconstructed (data at points with actual data were not changed). Only the first N M-SSA RCs were retained, where N was chosen to correspond to the number of modes that account for a certain fraction (we use 90%) of the full data set's variability. Remaining modes were regarded as noise and did not participate in the reconstruction. At the next iteration, the climatology based on a newly computed index time series was subtracted from the corresponding indices. The procedure was repeated until convergence, i.e., until in-filled data values stop changing

² This was one of the reasons to consider these as our primary subset.

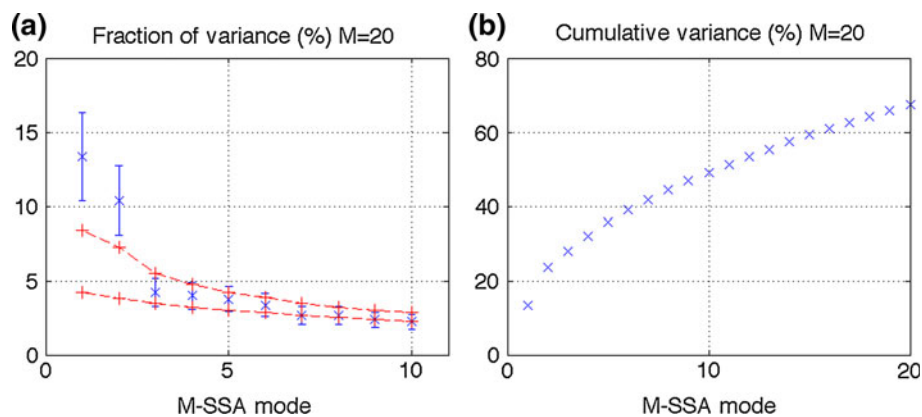


Fig. 1 M-SSA spectrum of the network of eight climate indices (see text): **a** Individual variances (%); **b** cumulative variance (% of the total). The M-SSA embedding dimension (window size) $M = 20$. The error bars in **a** are based on North et al. (1982) criterion, with the number of degrees of freedom set to 40, based on the decorrelation

within 10% of their standard error. Results of the data infilling were insensitive to the M-SSA window used, for window sizes $M = 10, 20, 30$, and 40.

We stress our caution in interpretation of statistical relationships found between in-filled indices in the first part of the twentieth century. These relationships will be considered real only if their counterparts exist in the late twentieth century.

2.3.3 Assessing statistical significance of stadium-wave-related cross-correlations

We tested statistical significance of M-SSA identified multidecadal modes (Sect. 3.1) and that of cross-correlations between interannual-to-interdecadal climate indices (Sect. 3.2) using two different stochastic models. The first model is a red-noise model fitted independently to each index considered. It has the form

$$x^{n+1} = ax^n + \sigma w, \quad (1)$$

where x^n is the simulated value of a given index at time n ; x^{n+1} is its value at time $n + 1$; w is a random number drawn from the standard normal distribution with zero mean and unit variance, while parameters a and σ are computed by linear regression. Model (1) produces surrogate time series characterized by the same lag-1 autocorrelation as the original (one-dimensional) data. However, by construction, true cross-correlations between surrogate time series of different indices are zero at any lag. Nonzero cross-correlations between these time series are artifacts of sampling due to finite length of the time series considered. Observed correlation between any pair of actual time series is considered to be statistically significant only if it lies outside of the envelope of correlation values predicted by

time scale of ~ 2.5 years. The +symbols and dashed lines in **a** represent the 95% spread of M-SSA eigenvalues base on 100 simulations of the eight-valued red-noise model (1), which assumes zero true correlations between the members of the eight-index set

multiple surrogate simulations of this pair generated by model (1).

The second model is a multivariate, two-level extension of model (1) (Penland 1989, 1996; Penland and Ghil 1993; Kravtsov et al. 2005). Construction of this second model was based on 15-index anomalies with respect to the multidecadal signal in order to concentrate on interannual-to-interdecadal, rather than multidecadal, variability. The model produces random realizations of the 15-valued climate-index anomalies with lag 0, 1, and 2-years covariance structure (including cross-correlations between the indices), which is statistically indistinguishable from the observed covariance structure. We used this model to test if cross-correlations between members of our climate network, computed over various sub-periods of the full time series (see Sects. 2.3.4, 3.2.2), exceeded sampling thresholds quantified by this model's surrogate realizations. In other words, we looked into non-stationary relationships between pairs of indices characterized by stronger-than-normal cross-index synchronization, depending on time segment analyzed. Our detailed methodology for this part of analysis is summarized in Sect. 2.3.4.

2.3.4 Testing for abnormal short-term synchronizations within the climate network

Definition of synchronization measure: Network connectivity. We first computed absolute values of cross-correlations between pairs of observed indices among all 15 members of our climate network over a 7-year-wide sliding window.³ This window size was chosen as a compromise between

³ The M-SSA-defined multidecadal signal was subtracted from the indices prior to computing cross-correlations.

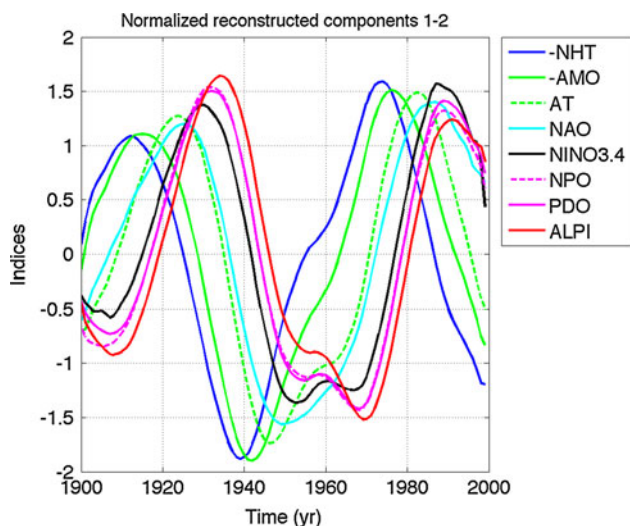


Fig. 2 Normalized reconstructed components (RCs) of the eight-index network. The RC time series shown have been normalized to have a unit variance. The indices are synchronized at, generally, non-zero lags, except for the indices NPO and PDO indices, whose rescaled RCs are virtually identical. Note that the reconstructions of *negative* NHT and AMO indices are displayed

maximizing the number of degrees of freedom in computing cross-correlations, while minimizing the time segment allotted in order to capture the characteristically brief duration of synchronization episodes (Tsonis et al. 2007; Swanson and Tsonis 2009). This procedure resulted in 100-year time series for each of the 105 cross-correlations among all possible pairs of the 15 indices; for each of the 100 years, we stored these cross-correlation values in the lower triangular part of the 15×15 cross-correlation matrix, with all other elements of this matrix being set to zero. We then defined the *connectivity* of our climate index network for a given year as the leading singular value of the Singular Value Decomposition (SVD; Press et al. 1994) of the above cross-correlation matrix, normalized by the square root of the total number of nonzero cross-correlations in this matrix (which equaled to 105 for the case of the full 15-index set). The connectivity defined in this way described a major fraction (typically larger than 80%; not shown) of the total squared cross-correlation within the network of climate indices, while providing a more robust measure of synchronization than the raw sum of squared correlations (cf. Swanson and Tsonis 2009). The maxima of connectivity time series defined local episodes of the climate network synchronization.

Identification of synchronizing subsets. Not all members of the climate network contribute equally to various synchronization episodes. To identify index subsets that maximize synchronization measure during such episodes, we employed the following re-sampling technique. We randomly drew a subset of K different indices (K varied from 6 to 10) from the full set of 15 indices and computed 100-year

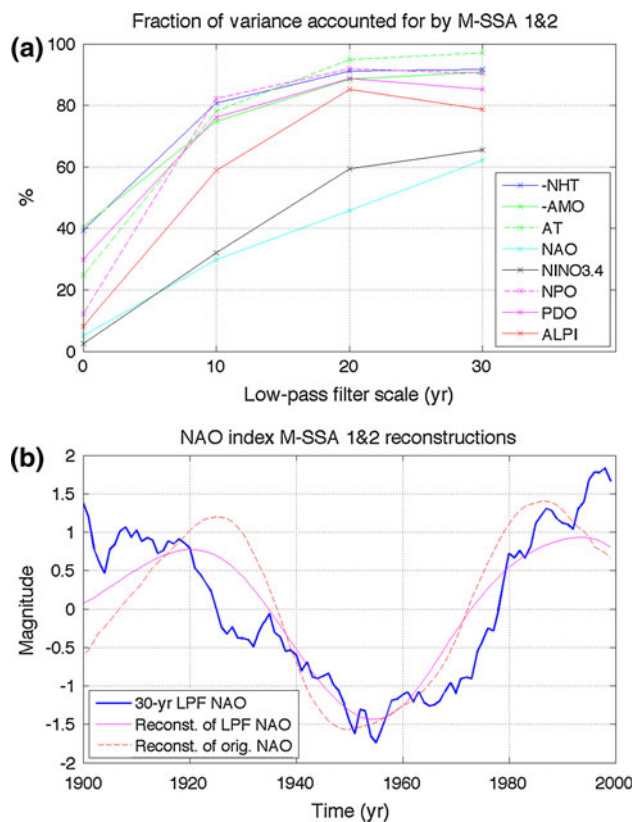


Fig. 3 **a** Fraction of each index variance (%) accounted for jointly by M-SSA modes 1 and 2, as a function of the low-pass filter time scale (years). Boxcar low-pass filtering has been applied to each index prior to the M-SSA analysis; the value of 0 corresponds to no prior low-pass filtering (the normalized RCs for this case are shown in Fig. 2), the values 10, 20, and 30 indicate 10-, 20-, and 30-years running-mean boxcar filtering. **b** Filtered NAO time series: heavy line—30-years running-mean boxcar filtered time series; *light line*—reconstruction based on M-SSA modes 1 and 2 of the 30-years low-pass filtered 8-index set; *dashed line*—reconstruction based on M-SSA modes 1 and 2 of the raw 8-index set (the same as in Fig. 2). All time series have been normalized to have unit variance

long connectivity time series based on this subset. We repeated this procedure 10,000 times, producing 10,000 100-year long connectivity time series. We then identified indices and years for which the connectivity value, based on at least one subset including this index, exceeded 95th and 99th percentiles of all connectivities that were based on the entire combined set of $(100 \text{ years}) \times (10,000 \text{ samples})$ surrogate connectivity values.

Statistical significance of synchronizations. To estimate statistical significance of synchronizations, we produced 1,000 random realizations of the 15-valued climate-index time series using the second stochastic model described in Sect. 2.3.3. While these surrogates mimic actual observed indices in the overall (climatological) covariance structure, they, by construction, are mathematically unaware of the magnitude and/or phasing of the multidecadal signal that was subtracted from the original data.

Connectivity time series for surrogate indices were then computed for each of the 1,000 realizations in the same way as for the original data. The 95th percentile of surrogate connectivity for each year defines the 5% a priori confidence levels. These levels should be used if one tests for some pre-defined years in the climate record being characterized by statistically significant synchronizations.

If no such a priori reasons exist, one has to use a posteriori confidence levels, which can be defined as follows. For each synthetic realization, we determine the maximum value of connectivity *over the entire 100-year period*; repetition of this procedure for all stochastic realizations results in 1,000 values of maximum surrogate connectivities. The 95th percentile of these maximum surrogate connectivities gives the 5% a posteriori confidence level for rejection of the null hypothesis stating that connectivity for each year is statistically the same as its true stationary value based on the correlation matrix computed over the entire 100-years period.

3 Results

3.1 Multidecadal “stadium wave”

Individual and cumulative variances of M-SSA modes for the main set of eight climate indices are shown in Fig. 1a and b. The leading pair of modes is well separated from the others according to the North et al. (1982) criterion. For the latter estimation, we have computed the number of effective temporal degrees of freedom N^* in our data set using the Bretherton et al. (1999) formula $N^* = N(1 - r^2)/(1 + r^2)$, where $N = 100$ is the length of the time series, and $r \approx 0.65$ is the maximum lag-1 autocorrelation among our set of eight indices. We will hereafter identify this statistically significant leading M-SSA pair with our climate “signal.” This dominant M-SSA pair *is unlikely to be due to random sampling of uncorrelated red-noise processes*, since it accounts for a substantially larger variance [exceeding the 97th percentile—upper dashed line in panel (a)] of the corresponding surrogate spectra generated by model (1).

Normalized RCs corresponding to joint M-SSA modes 1 and 2 are shown in Fig. 2; note that the reconstructions of *negative* NHT and AMO indices are displayed. Visual inspection of these RCs indicates they are dominated by a multidecadal climate signal with the time scale of about 50–80 years. Maximum-entropy spectral analysis (Press et al. 1994) of each of these RCs centers on the period of the broadband variability identified at about 64 years, indicative of long time scales associated with ocean dynamics.

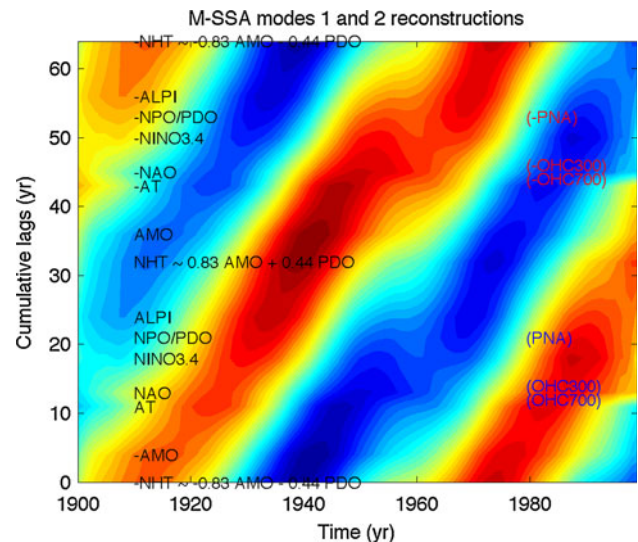


Fig. 4 Hoffmuller diagram of the “stadium-wave” propagation in the phase space of normalized RCs (for M-SSA modes 1 and 2 combined) of the extended set of 15 multidecadal indices (eight of the indices were described above, while the other seven indices are NPGO, OHC700, OHC300, PNA, WP, PMM, and AMM: see Figs. 5, 6 and text). For the additional indices, only the ones with substantial fraction of variance within leading pair of RCs (see Fig. 5) are shown. The horizontal cross-section in locations marked by index names shown on the *left* for the original eight indices, and on the *right* for the additional indices would represent time series of the corresponding index as plotted in Figs. 2 and 5. The indices are sorted from bottom to top of the figure in the order determined by cross-correlation analysis, while the vertical “distance” between each index equals the lead time of maximum cross-correlation between adjacent indices. Negative indices are also included to show one complete cycle (with the estimated period of 64 years) of the stadium-wave propagation

Our climate signal accounts for a substantial fraction of variance in several indices: NHT, AMO, PDO, and AT (see the values corresponding to zero low-pass filter time scale in Fig. 3a). This latter manifestation (AT) demonstrates a clear atmospheric response to ocean-induced multidecadal climate variations. On the other hand, fractional weakness of the multidecadally varying climate signal exists in NAO, ALPI, NPO, and NINO3.4; these are dominated by shorter-term fluctuations. Despite dominance of higher frequency behavior in the NAO, ALPI, NPO, and NINO3.4 modes, M-SSA still identifies within these indices a statistically significant, coherent multidecadal signal.

To demonstrate robustness of these results, we repeated M-SSA analysis using the running-mean boxcar low-pass filtered indices. We used three filters, with sliding window sizes of 10, 20, and 30 years. Ends of the data series are processed using shorter-filter-size running means and one-sided (or asymmetric) filters. Fraction of variance accounted for by the leading M-SSA pair of low-pass filtered data generally increases with scale of low-pass filter, the fractional increase of variance being most dramatic for ALPI, NPO, NAO, and NINO3.4 (Fig. 3a). Normalized

Table 2 The stadium-wave lags and their uncertainties (years) estimated using a bootstrap procedure (see text)

	–NHT → –AMO	AMO → AT	AT → NAO	NAO → NINO3.4	NINO3.4 → NPO/PDO	NPO/PDO → ALPI	ALPI → NHT
Mean	4.3	6.8	2.4	4.8	2.4	2.9	8.2
STD	0.5	0.4	1.3	1.6	1.1	1.3	1.2
1/2 95%	0.5	0.5	2.5	3.0	2.0	2.5	2.0

The time scale T of the observed stadium-wave cycle is given by twice-the-sum of the first-row values, while its standard uncertainty—by the square root of twice-the-sum of the second row’s squared values. These calculations result in the estimate of $T = 63 \pm 5$ year, consistent with the 64-years scale obtained in the 8-index (and 15-index) M-SSA analyses

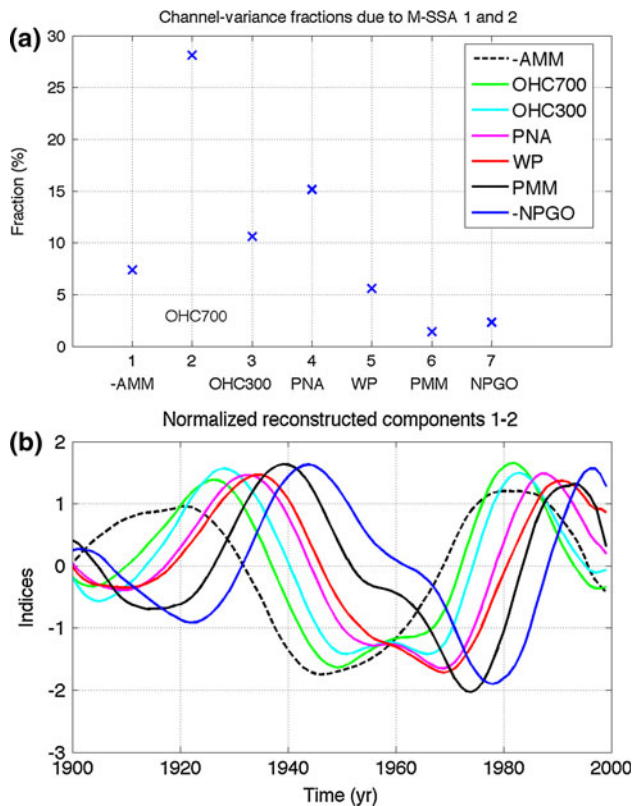


Fig. 5 The M-SSA results based on the analysis of the full 15-index data set. The quantities shown describe the statistics of the seven climatic indices considered in addition to the original 8-index set (see Figs. 2, 3). **a** Fraction of raw-index variance accounted for jointly by M-SSA modes 1 and 2 (Fig. 3a shows this quantity for the original eight indices). **b** The same as in Fig. 2, but for the additional seven climate indices (see **a** and figure legend for abbreviated index names)

RCs of the leading M-SSA mode of low-pass filtered indices are close to their counterparts obtained via M-SSA analysis of raw indices. Figure 3b shows this behavior in NAO. Note boxcar low-pass filtering is intrinsically characterized by a large phase error. This error is not entirely eliminated by M-SSA time–space covariance-based filtering, explaining shifts between the maxima and minima of filtered and raw RCs in Fig. 3b.

Figure 3b also illustrates well the distinction between M-SSA spatiotemporal filtering and time filtering,

underscoring the former’s advantage in analyzing climate data. Geophysical time series are typically characterized by presence of noise with substantial power in the low-frequency portion of the spectrum—the so-called red noise. Low-pass time filtering of a synthetic mixture of quasi-periodic time series with a strong red-noise component may erroneously reflect spurious low-frequency variability that has little to do with the shape of the actual quasi-periodic signal used to construct this time series. On the other hand, if the quasi-periodic signal is characterized by a coherent spatial structure that is distinct from noise, and if multivariate time series representing geographically diverse indices possessing this signal are available, separation of signal from noise is more robust (see Ghil et al. 2002 for further details). Note M-SSA reconstruction of low-pass filtered NAO index in Fig. 3b (light solid line) does not follow exactly excursions of the original low-pass filtered NAO index (heavy solid line). Deviations from purely temporal filtering reflect corrections resulting from M-SSA, which relies on cross-index lagged correlations of the dominant multidecadal signal.

To confirm a truly multivariate nature of the leading M-SSA signal, we employed the following bootstrap procedure. We randomly generated multiple (~15,000) combinations of the eight primary indices and applied M-SSA to each randomly assembled set, resulting in multiple sets of eight-valued RC time series—in some cases with certain indices being repeated, and others being omitted. For each of the eight indices, this procedure resulted in 10,000 sets of RC time series corresponding to leading M-SSA pairs of random index sets. Any statistical characteristic based on RCs of the original index set can also be computed for surrogate sets. The latter estimates can be used to assess the expected spread of statistical quantities computed. For example, the bootstrap-based estimate of dominant timescale of the leading M-SSA signal produces the mean value of 63 years, with the standard uncertainty of ± 5 years and 95% confidence interval close to twice the standard uncertainty. These estimates are thus consistent with results of the original eight-index analysis. *Robustness of bootstrap-based M-SSA reconstructions highlights lagged co-variability among the entire set of eight indices; the*

Fig. 6 The network of 15 climate indices: (1) M-SSA modes 1 and 2 RCs (blue); and (2) anomaly with respect to the corresponding RC (red). The blue and red lines give the raw climate index (detrended and normalized to have a unit variance). The abbreviated index names are given in panel captions

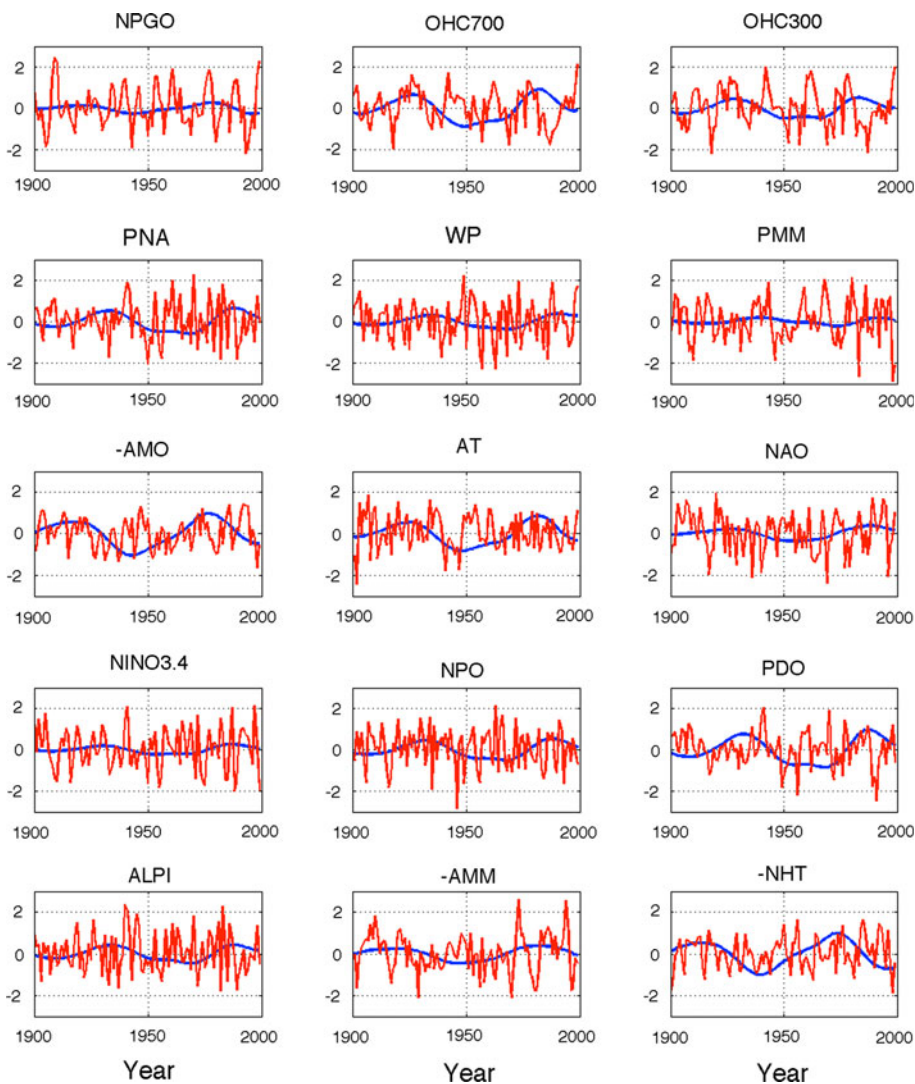


Table 3 Maximum lagged correlations (with corresponding lags) between climate indices computed over the full 100-years twentieth century record, as well as over its second half (1950–1999); the latter correlation values are shown in parentheses

	NPGO	OHC7	PNA	WP	AMO	NAO	NINO3.4	PDO
OHC3		0.9 (0.9), 0						
PMM	-0.54 (-0.52), 0							
NINO3.4			0.47 (0.54), -1	0.52 (0.49) , -1				
NPO				0.45 (0.46), -1			0.36 (0.48), 0	
PDO			0.75 (0.76), 0				0.41 (0.52), 1	
ALPI			0.77 (0.86), 0					0.55 (0.64), 0
AMM					0.54 (0.6) , 1	-0.57 (-0.52) , 0		
NHT			0.42 (0.44), 0		0.66 (0.74) , 0			

Only the correlations that are statistically significant at 5% a posteriori level for both of these periods—relative to the null hypothesis of zero correlation at any lag—are shown. Correlations equal or exceeding 0.5 (upon rounding up) are in bold font. The negative lags correspond to the column-member of an index pair leading its corresponding row member (“Column-members” arranged in the leftmost column; “row-members” arranged in the top row). For example, the maximum lagged correlation between NINO3.4 and PNA is equal to 0.47 (0.54 during the second half of the twentieth century), with NINO3.4 leading by 1 years

Fig. 7 M-SSA spectrum of the Pacific-centered multi-index set consisting of interdecadal anomalies (Fig. 6, red lines) of PNA, WP, NINO3.4, NPO, PDO, ALPI indices. The *bottom panel* shows raw time series of the NINO3.4 index and its RC based on M-SSA modes 1 and 2

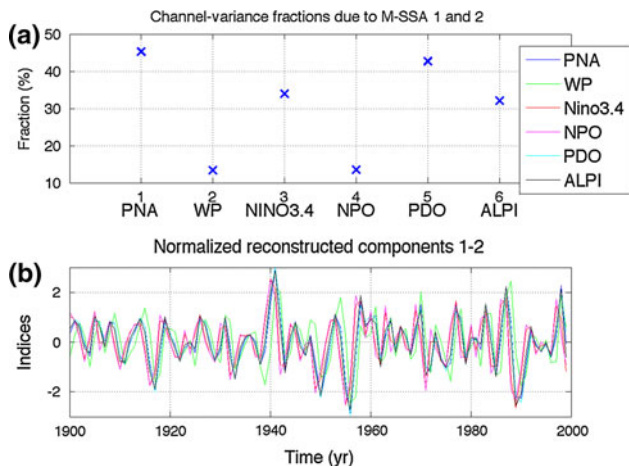
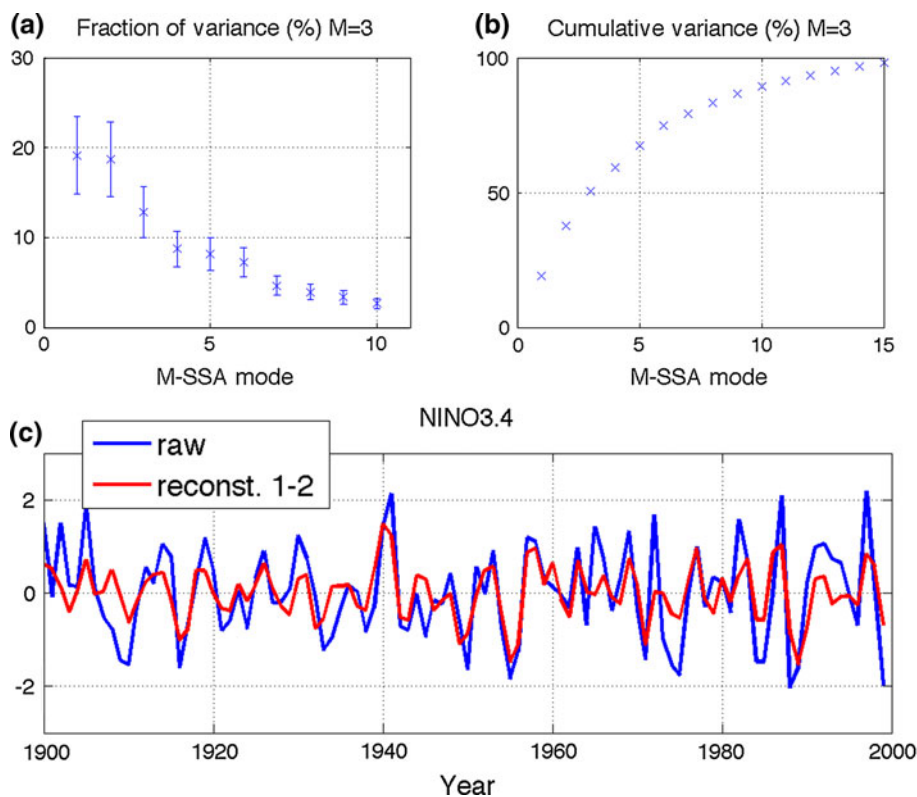


Fig. 8 The M-SSA results for the Pacific-centered index subset (see Fig. 7). See panel legend for abbreviated index names. Same conventions as in Fig. 5

leading M-SSA signal is not “dominated” by the variability in a particular M-SSA channel (say, NHT or AMO).

It is apparent from Fig. 2 that the climate-signal indices are correlated at nonzero lags, except for the normalized RCs 6 (NPO) and 7 (PDO), which turned out to be virtually identical. We objectively determined the lead–lag relationships between the RCs using the cross-correlation analysis (not shown), which unambiguously identifies, based on maximum cross-correlation, the order of RCs in the

“stadium wave” propagation across the phase space of the reconstructed climate indices. The phase of each RC in the stadium-wave sequence was computed by least-square fitting two-predictor time series $\{\sin(2\pi t/64), \cos(2\pi t/64)\}$, with t changing from 0 to 100, to each of the RCs. The following phase shifts between the “adjacent” RC pairs resulted:

- NHT → (4 years) → –AMO → (7 years) → AT
- (2 years) → NAO → (5 years) → NINO3.4
- (3 years) → NPO/PDO → (3 years) → ALPI
- (8 years) → NHT → (4 years) → AMO
- (7 years) → –AT → (2 years) → –NAO
- (5 years) → –NINO3.4 → (3 years)
- –NPO/PDO → (3 years) → –ALPI
- (8 years) → –NHT.

This “stadium wave” is summarized as a Hoffmuller diagram in Fig. 4. The complete cycle of the stadium wave has naturally a period of 64 years, and a bootstrap-based standard uncertainty of ± 5 years. The bootstrap-based estimates of the above lags and their uncertainties are listed in Table 2. Note that the fractional uncertainties vary considerably from one transition leg to another, due mainly to differences in mean duration of various transitions in the presence of fairly uniform absolute uncertainty. This describes the case for all but the NHT → –AMO and –AMO → + AT transitions, which involve indices strongly dominated by low-frequency

anomalies. Uncertainty of lag-time between these indices is smaller than that associated with index pairs involving noisier raw indices.

M-SSA results for the extended data set support those of the original stadium-wave analysis. Leading M-SSA modes 1 and 2 describe the multidecadal stadium wave, with no modification of phase relationships between the original eight indices (Figs. 4, 5). While all 15 indices reflect the dominant multidecadal signature, a stronger high-frequency component characterizes most of the seven complementary indices, rendering their fractional variance of the stadium-wave signal weak. Only those with strong fractional variance—PNA and OHC300/700—are displayed in the Hoffmuller diagram in Fig. 4. OHC700 exhibits the strongest fractional variance among the trio from the complementary indices, with a strong multidecadal component nearly in phase with that of the AT index. OHC300, on the other hand, exhibits a much lower fractional variance and its phasing is close to the NAO and NINO3.4 multidecadal signals. These observations invite speculation that ocean-heat-content variability at various depths within the subsurface North Pacific is governed by different dynamical processes related to indices within the stadium-wave network (see also discussion in Sect. 4.2).

3.2 Interannual-to-interdecadal variability

3.2.1 Variability unrelated to the stadium wave

To extract a residual signal from our 15 indices, we subtract the multidecadal signal (Fig. 6, blue lines) associated

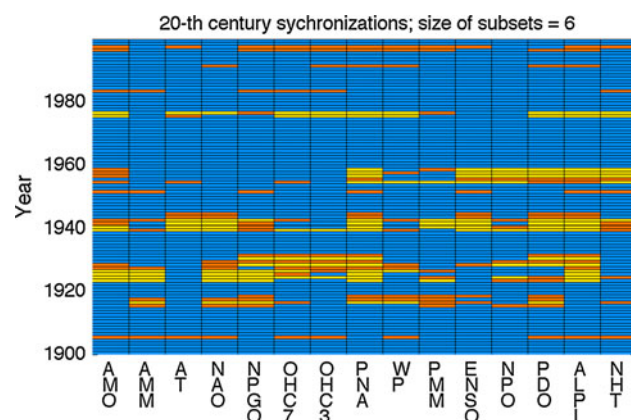


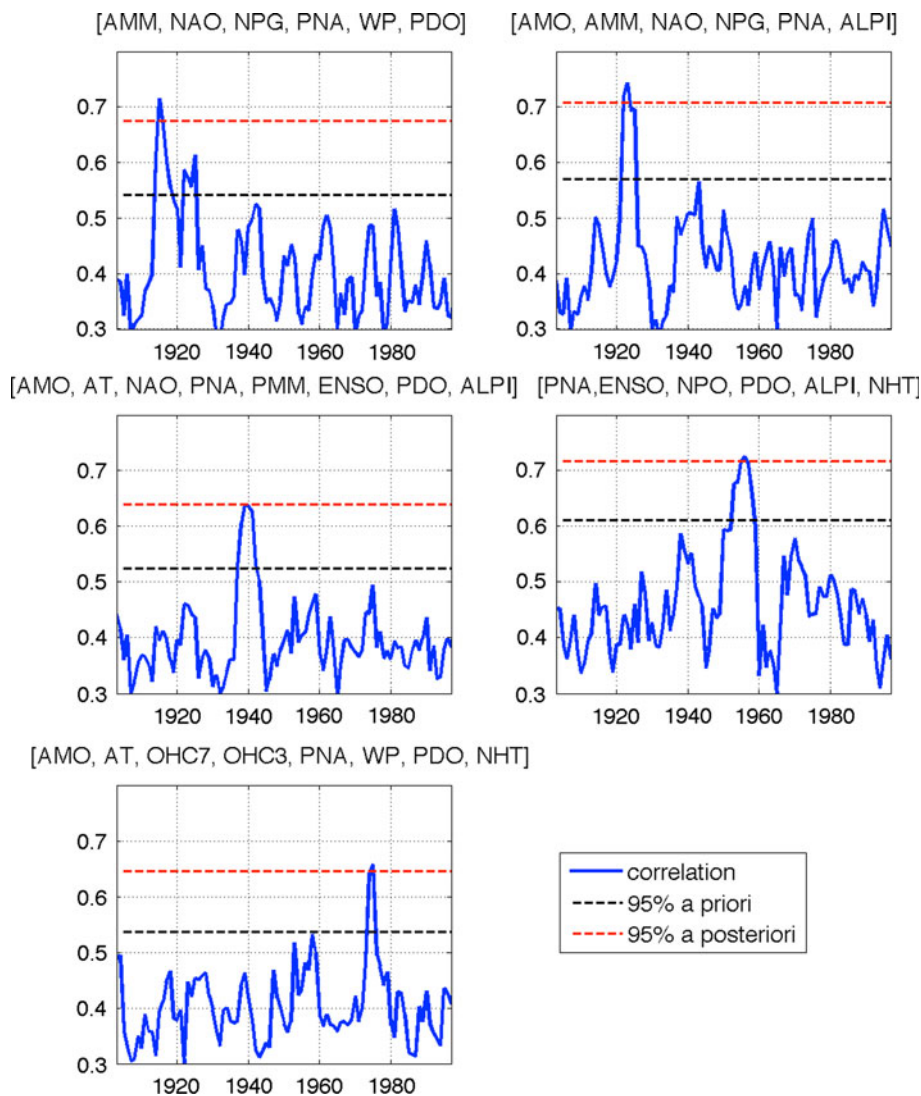
Fig. 9 Identification of index sub-networks. For a given year (on the vertical axis), bright yellow and orange cells indicate that there exists at least one six-index network that includes the index this cell represents (the indices are arranged along the horizontal axis), which is characterized by the network connectivity exceeding the 95th percentile of the connectivity for all possible 6-index networks and for all years; the yellow cells are characterized by the connectivity that exceeds the 99th percentile. See caption to Fig. 10 and text for the definition of network connectivity. The results for the subset sizes in the range from 4 to 8 (not shown) are analogous

with the stadium wave. This forms a network of climate indices (Fig. 6, red lines) that emphasizes higher-frequency, interannual-to-interdecadal climate variability. To study possible connections within this network, we first identify statistically significant (lagged) cross-correlations between index anomalies so computed (see Table 3). A posteriori significance levels were determined for each index pair using surrogate indices simulated by the red-noise model (1); see Sect. 2.3.3. We computed maximum lagged correlations (using the entire 100-year time series and over a range of all possible lags) for 100 sets of surrogate index time series, followed by sorting these correlations in ascending order, taking the 99th sorted values as the 1% significance level.

Analysis results of high-frequency variability of the residual signal point to a Pacific-centered subset of indices—PNA, PDO, ALPI, NINO3.4, WP, NPO—whose members exhibit behavior similar to one another (that is, they are correlated at zero or 1-year lags). Guided by this observation, we applied M-SSA to this select group of indices as a way to verify suspected relationships among them and to more graphically describe the cross-correlations between them. Relationships identified in cross-correlation analysis are corroborated by M-SSA results (Figs. 7, 8). In particular, we find NINO 3.4 and NPO correlated at zero lag; although the low fractional variance of NPO suggests caution regarding its degree of uncertainty. The same is true for WP (see Sect. 4.3). NINO3.4 and NPO lead others within this subset by 1 year, with the typical time scale of variability being on the order of 3–4 years. Based on time scale and spatial confinement, behavior of the Pacific-centered set has strong association with ENSO. These results are not surprising or novel. However, they do demonstrate that the network approach we took is sound, as it corroborates previous findings by other researchers on ENSO teleconnections.

Another statistically significant cross-index relationship identified includes that between OHC700 and OHC300, which is, of course, not unexpected given the similar nature of the two indices. There is also the anti-correlation between the members of PMM/NPGO pair. Both of the latter indices are dominated by interdecadal anomalies (see Fig. 6). There is also a statistically significant positive simultaneous correlation between the interdecadal anomalies of AMO and NHT indices, demonstrating that the North Atlantic decadal-to-interdecadal SST anomalies directly explain a significant fraction of the NHT decadal-to-interdecadal variability. Finally, the cross-correlation analysis identifies substantial co-variability within the Atlantic-based index trio: AMM, AMO, and NAO, thus suggesting interesting dynamical connections among various components of the coupled AMOC system.

Fig. 10 The time series of index connectivity for the sub-networks identified in Fig. 9. The indices comprising each subset are listed in the caption of each panel. The measure of connectivity used here is the leading singular value of the lower triangular part of the index cross-correlation matrices computed over the 7-years sliding window. The *horizontal dashed lines* indicate 5% a priori and a posteriori confidence levels based on the linear stochastic model that reproduces the *climatological* cross-correlations between the indices



3.2.2 Effects of the stadium wave on interannual-to-interdecadal climate anomalies

Next we wish to see if collective behavior of higher-frequency variability of the residual signal has a relationship with the stadium-wave multidecadal signal. This line of inquiry was motivated by work of Tsonis et al. (2007) and Swanson and Tsonis (2009). These authors identified five intervals within the twentieth century during which certain climate indices abnormally synchronized—matching with strong statistical significance in both rhythm and phase of their interannual variability; the five intervals were centered at the years 1916, 1923, 1940, 1957, and 1976. Three of five synchronizations (1916, 1940, 1976) coincided with hemispheric climate-regime shifts, which were characterized by a switch between distinct atmospheric and oceanic circulation patterns, a reversal of NHT trend, and by an altered character of ENSO variability (intensity and dominant timescale of variability (Federov and Philander 2000;

Dong et al. 2006; Kravtsov 2011, among others). As the authors had expected, based on synchronized chaos theory, these “successful” synchronizations (i.e., the ones preceding climate shifts) were accompanied by increased network coupling defined via the climate index network’s phase-prediction measure. Two synchronizations *not* leading a climate-regime shift were *not* accompanied by increased network coupling. We observe here that the timing of the regime shifts has a multidecadal pace, consistent with the stadium wave; we are thus motivated to further explore synchronizations in our extended (compared to Tsonis et al.) climate network.

We first determine the years of abnormal synchronizations and synchronizing subsets within the main 15-index set using the methodology described in Sect. 2.3.4. Results presented in Fig. 9 identify five time bands characterized by high connectivity values among the subsets of the full 15-index set; these bands are centered at years 1916, 1923, 1940, 1957 and 1976—thus consistent with studies by

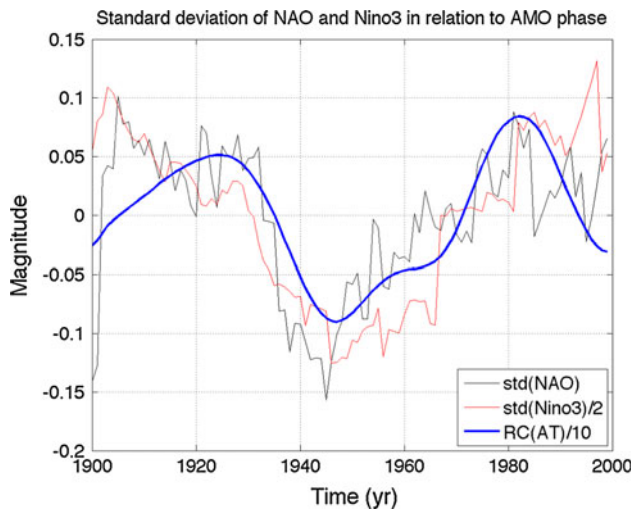


Fig. 11 Anomalies (with respect to the mean value of 1) of NAO (light black line) and Nino3 (light red line) standard deviations, along with the M-SSA mode's 1–2 RC of AT index (heavy blue line; this line is the same as that in the middle panel of Fig. 7, but multiplied here by a factor of 0.1). The Nino3 standard-deviation anomaly has been scaled by a factor of 0.5 for easier visual analysis. The standard deviations for each index shown were computed over the 31-years-wide sliding window

Tsonis et al. Synchronizing subsets comprise the following indices (based on the 99th percentile of re-sampled sub-networks; see Sect. 2.3.4): AMM, NAO, NPGO, PNA, WP, PDO for the 1916 subset; AMO, AMM, NAO, NPGO, PNA, ALPI for the 1923 subset; AMO, AT, NAO, PNA, PMM, ENSO, PDO, ALPI for the 1940 subset; PNA, ENSO, NPO, PDO, ALPI, NHT for the 1957 subset; and AMO, AT, NAO, OHC700, OHC300, PNA, WP, PDO, ALPI, NHT for the 1976 subset. Connectivity time series computed for each subset exhibit statistically significant maxima during corresponding time bands (Fig. 10). While the statistical significance of connectivity maxima drops substantially if one accounts for degrees of freedom associated with possibility of drawing multiple index subsets of a given size from the full set of 15 indices, all of the connectivity maxima in Fig. 10 still exceed the 5% a priori levels in this case (not shown). The use of a priori levels may, in fact, be more appropriate for successful synchronization episodes, given the evidence for regime shifts and predictions of synchronized chaos theory that rationalize expected synchronizations preceding these shifts (Tsonis et al. 2007; Swanson and Tsonis 2009).

Our results here provide a more detailed picture of the 1916, 1940 and 1976 (“successful”) synchronizations and expose differences between these three “successful” and two “unsuccessful” episodes (i.e., 1923 and 1957) in terms of index membership of corresponding synchronizing subsets. In particular, the 1957 episode is confined mostly within the Pacific; while the Atlantic reflects a greater

influence during the 1923 synchronization. Successful synchronizations tend toward a more symmetrical contribution from both the Atlantic and Pacific sectors and PNA participates in all synchronizations. Note that timing between successful synchronizations, shifts between alternating periods of enhanced and diminished interannual variance of ENSO and NAO (Fig. 11), and the stadium-wave tempo share similar pace, thus suggesting possible stadium-wave influence on synchronizations within the climate network.

In summary, while our research on the interrelationships between the multidecadal signal and higher-frequency variability continues, the above results suggest that the major synchronization episodes and regime shifts of interannual-to-decadal climate variability all over the world are paced by the multidecadal climate variations originating in the North Atlantic (see Sect. 4).

4 Summary and discussion

4.1 Summary

We considered the Northern Hemisphere's climate variability in a network of well-known indices describing climatic phenomena all over the Northern Hemisphere (NH). Our network approach—via data compression to a subspace of dynamically and geographically distinct indices—provides means to establish rigorous estimates of uncertainty associated with multidecadal variability observed in the instrumental climate records and to address the question of how likely these observed multidecadal teleconnections are to be due merely to random sampling of uncorrelated red-noise time series. Multi-channel Singular Spectrum Analysis (M-SSA) of this network (Figs. 1, 2, 3, 4, 5) identifies the dominant signal with a time scale of 50–80 years, which propagates through the phase space of the indices considered as the “stadium wave” (Fig. 4; Table 2). In Sect. 4.2 below, we interpret this stadium wave in terms of the sequence of atmospheric and multi-year-lagged oceanic teleconnections originating from the Atlantic Multidecadal Oscillation (AMO)—an extensively studied intrinsic oceanic mode associated with the variability of Meridional Overturning Circulation (MOC). The stadium-wave propagation is reflected in the NH area-averaged surface temperature signal, which explains, by inference, at least a large fraction of the multidecadal non-uniformity of the observed global surface temperature warming in the twentieth century.

In Sect. 3.2, we decomposed the climate indices into the stadium-wave multidecadal and shorter-term residual variability (Fig. 6). The dominant residual signal is the Pacific-centered suite of interannual ENSO teleconnections

(Table 3; Figs. 7, 8). Results summarized in Table 3 also show that a major portion of the shorter-term (with respect to the stadium wave time scale), decadal-to-interdecadal variations of NH surface temperature (NHT) is directly related to the corresponding variability of the North Atlantic sea-surface temperature (SST). In combination with the inferred AMO/NHT stadium-wave connections, these findings imply that the North Atlantic SSTs exert a strong influence on the hemispheric climate across the entire range of time scales considered.

One of the most intriguing findings that came out of our analysis is the apparent connection between the hemispheric climate regime induced by the stadium-wave dynamics and the character of interannual climate variability. In particular, the pacing of the stadium wave is consistent with the timing between the episodes of abnormal synchronization of Atlantic/Pacific teleconnections (Figs. 9, 10, 11). The termination of these synchronization episodes coincided with hemispheric climate-regime shifts characterized by the switch of the climate regime from the one characterized by the high ENSO variance (pre-1939), to the one with low ENSO variance (1939–1976), and back to the high ENSO variance regime (post-1976); see Fig. 11. The NAO interannual variance exhibits similar multidecadal variability, as shown in Fig. 11, suggesting Pacific–Atlantic feedback.

Thus, results presented in this note suggest that AMO teleconnections, as captured by our stadium-wave, have implications for decadal-scale climate-signal attribution and prediction—both significant to the developing field of climate research.

4.2 Discussion: Stadium-wave's hemispheric propagation

Statistical results developed above describe only co-variability within the climate-index network, not causality. We interpret these results based on a wide variety of observational and modeling studies, which rationalize the existence of the multidecadal climate signal—Atlantic Multidecadal Oscillation (AMO)—that originates dynamically in the North Atlantic Ocean and propagates throughout the Northern Hemisphere via a suite of atmospheric and oceanic processes, or the stadium wave.

Inconsistent modeling results foil simple narrative, with dependency of the simulated low-frequency climate variability upon model configuration, initialization, and spatial resolution (Metzger and Hurlburt 2001; Yualeva et al. 2001; Kushnir et al. 2002; Kelly and Dong 2004; Minobe et al. 2008). Instrumental records, on the other hand, are short, and while they have been shown to reflect a multidecadal signature (Folland et al. 1986; Kushnir 1994; Schlesinger and Ramankutty 1994; Delworth and Mann

2000), their direct interpretation is difficult. These collective challenges are mollified somewhat by observations from proxy records (Mann et al. 1995, 1998; Black et al. 1999; Shabalova and Weber 1999; Gray et al. 2004; Klyashtorin and Lyubushin 2007), which do indicate the tendency of a diverse collection of paleo-climate indices to exhibit climate variability on a shared multidecadal cadence—a finding similar to ours.

Despite caveats of model studies, their results are instructive in context of our proposed stadium wave, describing potential mechanisms for climate-signal generation and its subsequent hemispheric propagation. Hypotheses for AMO origin often find common ground in the suspicion that AMOC plays a nontrivial role in generating and setting the pace of the AMO. Many models produce intrinsic interdecadal and multidecadal variability (Delworth et al. 1993; Delworth et al. 1997; Timmermann et al. 1998; Cubasch and Voss 2000; Delworth and Greatbatch 2000; Hilmer and Jung 2000; Eden and Jung 2001; Shindell et al. 2001; Bryden et al. 2005; Getzlaff et al. 2005; Delworth and Dixon 2006; Latif et al. 2004, 2006; Dima and Lohmann 2007; Vellinga and Wu 2004; Delworth et al. 2007; Msadek et al. 2010a), although mechanisms behind the observed variations are still a matter of debate. Models with periodicities and boreal-winter atmospheric projections closest to observation seem to require a deep or interactive ocean (Knight et al. 2005; Msadek et al. 2010b), underscoring the hypothesized AMO link to AMOC-related ocean dynamics.

The Atlantic SST Dipole—an index based on inter-hemispheric Atlantic SST anomalies—is thought to reflect AMOC-forced SST fluctuations related to the AMO (Black et al. 1999; Keenlyside et al. 2008). Motivated by this observation, we added the dipole to our MSSA mix of indices. What we found was the SST-dipole-index RC identical in phasing to that of the NHT RC. NHT leads AMO by about 4 years—and so does AMOC, according to the SST Dipole proxy. We also experimented with the addition of a paleo-proxy for the SST Dipole (*G. bulloides*; see Black et al. 1999) to our MSSA collection of indices and found, once again, the phasing identical to the NHT RC. Considering the collective evidence—the dipole phasing, paleo-proxy phasing, and model studies, we suggest the AMOC indeed plays a significant role in generating the AMO.

4.2.1 The AMOC generated multidecadal SST signal and its relationship with the overlying atmosphere

Bjerknes (1964) argued that long-term top-of-the-atmosphere radiative balance remains fairly constant and so is the total poleward heat transport accomplished by ocean and atmosphere. Therefore, when one vehicle of poleward

heat transport weakens, the other strengthens to compensate, the phenomenon known as “Bjerknes Compensation.” Shaffrey and Sutton (2006) and Van der Swaluw et al. (2007) showed via modeling studies that Bjerknes compensation is operative in the northern North Atlantic Ocean, with maximum expression between 60°N and 80°N, on decadal and longer time scales. Note that the AMO SST index reflects the ocean surface signature of AMOC multidecadal variability and is thus not representative of the oceanic heat transport, which may exhibit decadal delays with respect to SST due to oceanic dynamical inertia (see, for example, Marshall et al. 2001a, b; Kravtsov et al. 2008, and references therein). Consistent with this notion, our results find that the –AMO index leads the AT index (related to atmospheric mass and heat transport) and NAO index (related to atmospheric mass) by 7 and 9 years, respectively. This implies that oceanic/atmospheric heat transport has a minimum/maximum a few years after peak negative SST anomalies in the North Atlantic, with atmospheric transport causing NAO to peak shortly after. These timings are consistent with Msadek et al. (2010b).

4.2.2 Potential mechanisms transmitting the multidecadal SST signal to the overlying atmosphere

Mechanisms behind the North Atlantic SST anomalies' influence on the overlying atmosphere on decadal-to-multidecadal time scales, as suggested by the above energy-balance considerations, remain the subject of extensive research. For example, Kelly and Dong (2004) and Dong and Kelly (2004) found that strong basin-scale westerlies in both the North Atlantic and North Pacific co-occur with anomalously high ocean heat content and strong negative heat flux (out of the ocean) in the western-boundary currents and their extensions (see also Hansen and Bedzek 1996; Sutton and Allen 1997; McCartney 1997; Marshall et al. 2001a). These results argue that there exists a positive, reinforcing feedback on SST anomalies through oceanic modification of overlying atmospheric circulation (Palmer and Sun 1985; Latif and Barnett 1994, 1996; Kushnir and Held 1996; Rodwell et al. 1999; Latif et al. 2000; Mehta et al. 2000; Robertson et al. 2000; Czaja and Frankignoul 2002; Wu and Gordon 2002; Sutton and Hodson 2003; Wu and Rodwell 2004; Xie 2004; Xie and Carton 2004). Note, however, that details of this response are sensitive to the location of the heat source with respect to the mid-latitude storm track (Peng et al. 1997; Peng and Whitaker 1999; Peng and Robinson 2001; Czaja and Marshall 2001; Peng et al. 2002; Nakamura et al. 2004; Xie 2004; Minobe et al. 2008), with substantial inconsistencies among the models—see Kushnir et al. (2002) for a review and Msadek et al. 2010b.

4.2.3 Generation of the hemispheric response: Atlantic–Pacific teleconnections

A variety of models with prescribed AMO-related SSTs show consistent hemispheric response (Delworth et al. 1993; Kushnir 1994; Hakkinen 1999; Delworth and Mann 2000; Sutton and Hodson 2003; Sutton and Hodson 2005; Knight et al. 2006; Grosfeld et al. 2007; Sutton and Hodson 2007). Longitudinal and latitudinal migrations of atmospheric centers-of-action (COA) appear to govern circumpolar communication of regionally generated climate signals (Kirov and Georgieva 2002; Polonsky et al. 2004; Grosfeld et al. 2007; Dima and Lohmann 2007; Msadek et al. 2010b). Dominant direction of wind flow across the entire range of longitudes (AT) and inter-basin connectivity modify accordingly: Wang et al. (2007) find that COA migrations generate intervals when climate patterns over the North Pacific and over the Eurasian continent upstream are linked, as are regions downstream, via an enhanced PNA and an eastwardly extended jet stream. During these time segments of enhanced circum-hemispheric stationary wave patterns, ENSO influence on ALPI becomes secondary to mid-latitude dynamics (Wang et al. 2007). Latitudinal shifts in atmospheric COAs—strongly influenced by NPO/WP patterns (Sugimoto and Hanawa 2009; Frankignoul et al. 2011)—have also been shown to influence interdecadal-scale migrations of western-boundary-current extensions (oceanic-gyre frontal boundaries), with impact on western-boundary dynamics and air-sea interaction (Kwon et al. 2010; Frankignoul et al. 2011). These sets of processes, after accounting for interannual delays due to oceanic dynamical adjustment, rationalize the sequence of the hemispheric and Pacific centered indices in our stadium wave.

Other proposed mechanisms for conveying an Atlantic-born climate signal to the North Pacific include stability changes within the tropical thermocline (Dong and Sutton 2005; Dong et al. 2006; Zhang and Delworth 2005, 2007; Zhang et al. 2007; Timmermann et al. 2007) and latitudinal shifts of Intertropical Convergence Zones (ITCZ) (Vellinga and Wood 2002; Vellinga and Wu 2004; Vimont and Kossin 2007). Tropical Pacific multidecadal changes may further modify the North Pacific response to AMO via an atmospheric bridge (Lau and Nath 1994; Deser and Blackmon 1995; Zhang et al. 1996). All the while, the AMOC continues its quasi-oscillatory behavior; the related AMO teleconnection sequence evolves accordingly. Possibly the Pacific communicates back to the Atlantic via tropical connections; this hypothesis will be addressed in a future study.

4.3 Discussion: Interannual-to-interdecadal variability

Our results support the notion that higher-frequency variability, especially in the Pacific, is modified according to polarity of the multidecadal signal. A Pacific subset—PNA, PDO, ALPI, NINO3.4, WP, and NPO—thus becomes a focus for this multidecadally alternating interannual-to-interdecadal behavior (see Table 3; Fig. 8). Perhaps striking is the comparatively low fractional variance displayed by the NPO and its upper-atmosphere counterpart—WP—both of which show significant correlation with NINO3.4. Potentially relevant to this conundrum is the observation of a non-stationary relationship between the NPO and ENSO (Wang et al. 2007), with ENSO-related signal in the ALPI strengthening and weakening at a multidecadal pacing and affecting the hemispheric interconnectedness of mid-latitude Pacific-centered indices, including NPO and WP.

Absent from our Pacific grouping are NPGO and PMM, which other studies have linked to ENSO by way of NPO. Our results suggest a strong negative relationship between higher-frequency behavior of NPGO and PMM, but not a significant relationship between NPGO and either NINO3.4 or NPO, in contrast to some other studies (Di Lorenzo et al. 2009). This discrepancy may be due to differences underpinning methods and data used. For example, different authors used different versions of the NPO index (Di Lorenzo et al. 2008; Chhak and DiLorenzo 2007; Ceballos et al. 2009; Di Lorenzo et al. 2009; and Di Lorenzo et al. 2010), with possibly large ensuing differences in the NPO–NPGO correlation. The same is true for various versions of ENSO related indices. Further potential explanations for our finding no significant correlations between NPO and PMM, as well as ENSO and PMM, include the seasonal dependence of these cross-correlations missed in our boreal-winter index analysis, and likely nonlinearity of the ENSO–PMM connection (Vimont et al. 2001, 2003a, b; Chiang and Vimont 2004; Chang et al. 2007), which is not optimally described by linear correlation measures.

In conclusion, dynamics presented above—potential mechanisms underlying stadium-wave dynamics and related dynamics on interdecadal time scales—are topics of active and controversial research, reliant upon technological leaps in data retrieval and computer modeling to advance them toward consensus. We suggest momentum on these investigations is building and that our statistical analysis is consistent with these emerging hypotheses.

Acknowledgments We thank S. Minobe for a useful feedback on aspects of this study, and three anonymous reviewers for comments on an earlier version of the manuscript, which helped clarify the presentation. This research was supported by the Office of Science (BER), US Department of Energy (DOE) grant DE-FG02-07ER64428, NSF grant ATM-0852459 (SK), and NSF grant AGS-0902564.

References

- Alexander MA, Deser C (1995) A mechanism for the recurrence of wintertime midlatitude SST anomalies. *J Phys Oceanogr* 25:122–137
- Beamish RJ, Neville CM, Cass AJ (1997) Production of Fraser River sockeye salmon (*Oncorhynchus nerka*) in relation to decadal-scale changes in the climate and the ocean. *Can J Fish Aquat Sci* 56:516–526
- Beckers J, Rixen M (2003) EOF calculations and data filling from incomplete oceanographic data sets. *J Atmos Ocean Technol* 20:1839–1856. doi:10.1175/1520-0426(2003)
- Bell GD, Halpert MS (1995) Atlas of intraseasonal and interannual variability, 1986–1993. NOAA Atlas no. 12. Climate Prediction Center, NOAA/NWS/NMC, Washington DC. Request copy via e-mail from Gerald Bell at wd52gb@hp32.wvb.noaa.gov
- Bjerknes J (1964) Atlantic air–sea interaction. *Advances in geophysics* 10. Academic Press, New York, pp 1–82
- Black D, Peterson LC, Overpeck JT, Kaplan A, Evans MN, Kashgarian M (1999) Eight centuries of North Atlantic Ocean atmosphere variability. *Science* 286:1709–1713. doi:10.1126/science.286.5445.1709
- Bretherton CS, Widmann M, Dymnikov VP, Wallace JM, Blade I (1999) The effective number of spatial degrees of freedom of a time-varying field. *J Clim* 12:1990–2009
- Broomhead DS, King GP (1986) Extracting qualitative dynamics from experimental data. *Phys D* 20:217–236
- Bryden H, Longworth HR, Cunningham SA (2005) Slowing of the Atlantic meridional overturning circulation at 25°N. *Nature* 438:655–657. doi:10.1038/nature04385
- Ceballos LI, Di Lorenzo E, Hoyos CD, Schneider N, Taguchi B (2009) North Pacific Gyre Oscillation synchronizes climate fluctuations in the eastern and western boundary systems. *J Clim* 22:5163–5174
- Chang P, Zhang Li, Saravanan R, Vimont DJ, Chiang JCH, Link Ji, Seidel H, Tippett MK (2007) Pacific meridional mode and El Niño–Southern Oscillation. *Geophys Res Lett* 34:L16608. doi:10.1029/2007GL030302
- Chhak K, Di Lorenzo E (2007) Decadal variations in the California current upwelling cells. *Geophys Res Lett* 34:L14604. doi:10.1029/2007GL030203
- Chiang JCH, Vimont D (2004) Analogous Pacific and Atlantic meridional modes of tropical atmosphere–ocean variability. *J Clim* 17:4143–4158. doi:10.1175/JCLI4953.1
- Cubasch U, Voss R (2000) The influence of total solar irradiance on climate. *Space Sci Rev* 94:185–198. doi:10.1023/A:1026719322987
- Czaja A, Frankignoul C (2002) Observed impact of atlantic SST anomalies on the north atlantic oscillation. *J Clim* 15:606–623
- Czaja A, Marshall J (2001) Observations of atmosphere–ocean coupling in the North Atlantic. *OJR Meteorol Soc* 27:1893–1916. doi:10.1002/qj.49712757603
- Delworth TL, Dixon KW (2006) Have anthropogenic aerosols delayed a greenhouse gas-induced weakening of the North Atlantic thermohaline circulation? *Geophys Res Lett* 33:L02606. doi:10.1029/2005GL024980
- Delworth TL, Greatbatch RJ (2000) Multidecadal thermohaline circulation variability driven by atmospheric surface flux forcing. *J Clim* 13:1481–1495
- Delworth TL, Mann ME (2000) Observed and simulated multidecadal variability in the Northern Hemisphere. *Clim Dyn* 16:661–676. doi:10.1007/s003820000075
- Delworth TL, Manabe S, Stouffer RJ (1993) Interdecadal variations of the thermohaline circulation in a coupled ocean–atmosphere model. *J Clim* 6:1993–2011

- Delworth TL, Manabe S, Stouffer RJ (1997) Multidecadal climate variability in the Greenland Sea and surrounding regions: a coupled mode simulation. *Geophys Res Lett* 24(3):96GL03927: 257–260
- Delworth TL, Zhang R, Mann ME (2007) Decadal to centennial variability of the Atlantic from observations and models. In: Schmittner A, Chiang JCH, Hemming SR (eds) Past and future changes of the oceans meridional overturning circulation: mechanisms and impacts. Geophysical monograph series 173, American geophysical union, pp 131–148
- Deser C, Blackmon ML (1995) On the relationship between tropical and north pacific sea surface temperature variations. *J Clim* 8:1677–1680
- Di Lorenzo E, Schneider N, Cobb KM, Franks PJS, Chhak K, Miller AJ, McWilliams JC, Bograd SJ, Arango H, Curchitser E, Powell TM (2008) North Pacific Gyre Oscillation links ocean climate and ecosystem change. *Geophys Res Lett* 35:L08607. doi: [10.1029/2007GL032838](https://doi.org/10.1029/2007GL032838)
- Di Lorenzo E, Fiechter J, Schneider N, Miller AJ, Franks PJS, Bograd SJ, Moore A, Thomas A, Crawford W, Pena A, Herman AJ (2009) Nutrient and salinity decadal variations in the central and eastern North Pacific. *Geophys Res Lett* 36:L14601. doi: [10.1029/2009GL038261](https://doi.org/10.1029/2009GL038261)
- Di Lorenzo E, Cobb KM, Furtado JC, Schneider N, Anderson BT, Bracco A, Alexander MA, Vimont DJ (2010) Central Pacific El Niño and decadal climate change in the North Pacific Ocean. *Nat Geosci* 3(11):762–765. doi: [10.1038/NNGEO984](https://doi.org/10.1038/NNGEO984)
- Dima M, Lohmann G (2007) A hemispheric mechanism for the atlantic multidecadal oscillation. *J Clim* 20:2706–2719. doi: [10.1175/JCLI14174.1](https://doi.org/10.1175/JCLI14174.1)
- Dong S, Kelly K (2004) Heat budget in the Gulf Stream Region: the importance of heat storage and advection. *J Phys Ocean* 34:1214–1231
- Dong BW, Sutton RT (2002) Adjustment of the coupled ocean-atmosphere system to a sudden change in the Thermohaline Circulation. *Geophys Res Lett* 29(15). doi: [10.1029/2002GL015229](https://doi.org/10.1029/2002GL015229)
- Dong BW, Sutton RT (2005) Mechanism of interdecadal thermohaline circulation variability in a coupled ocean-atmosphere GCM. *J Clim* 18:1117–1135. doi: [10.1175/JCLI3328.1](https://doi.org/10.1175/JCLI3328.1)
- Dong BW, Sutton RT (2007) Enhancement of ENSO variability by a weakened atlantic thermohaline circulation in a coupled GCM. *J Clim* 20:4920–4939. doi: [10.1175/JCLI4282.1](https://doi.org/10.1175/JCLI4282.1)
- Dong BW, Sutton RT, Scaife AA (2006) Multidecadal modulation of El Niño Southern Oscillation (ENSO) variance by Atlantic Ocean sea surface temperatures. *Geophys Res Lett* 33:L08705. doi: [10.1029/2006GL025766](https://doi.org/10.1029/2006GL025766)
- Eden C, Jung T (2001) North Atlantic interdecadal variability: oceanic response to the North Atlantic Oscillation. *J Clim* 14:676–691
- Elsner JB, Tsonis AA (1996) Singular spectrum analysis: a new tool in time series analysis. Springer, New York
- Enfield DB, Mestas-Núñez AM (1999) Multiscale variabilities in global sea surface temperatures and their relationships with tropospheric climate patterns. *J Clim* 12:2719–2733
- Enfield DB, Mestas-Núñez AM, Trimble PJ (2001) The atlantic multidecadal oscillation and its relation to rainfall and river flows in the continental US. *Geophys Res Lett* 28:277–280
- Federov A, Philander SG (2000) Is El Niño changing? *Science* 288:1997–2002. doi: [10.1126/science.288.5473.1997](https://doi.org/10.1126/science.288.5473.1997)
- Folland CK, Palmer TN, Parker DE (1986) Sahel rainfall and worldwide sea temperature 1901–1985. *Nature* 320:602–607
- Frankignoul C, Sennechael N, Kwon Y, Alexander M (2011) Influence of the Meridional Shifts of the Kuroshio and the Oyashio extensions on the atmospheric circulation. *J Clim* 24:762–777. doi: [10.1175/2010JCLI3731.1](https://doi.org/10.1175/2010JCLI3731.1)
- Getzlaff J, Böning CW, Eden C, Biastock A (2005) Signal propagation related to the North Atlantic overturning. *Geophys Res Lett* 32. doi: [10.1029/2004GL021002](https://doi.org/10.1029/2004GL021002)
- Ghil M, Vautard R (1991) Interdecadal oscillations and the warming trend in global temperature time series. *Nature* 305:324–327
- Ghil M, Allen MR, Dettinger MD, Ide K, Kondrashov D, Mann ME, Robertson AW, Saunders A, Tian Y, Varadi F, Yiou P (2002) Advanced spectral methods for climatic time series. *Rev Geophys* 40(1):3.1–3.41. doi: [10.1029/2000GR000092](https://doi.org/10.1029/2000GR000092)
- Girs AA (1971) Multiyear oscillations of atmospheric circulation and long-term meteorological forecasts. *L Gidrometeroizdat* (in Russian)
- Gray ST, Graumlich LJ, Betancourt JL, Pederson GT (2004) A tree-ring based reconstruction of the Atlantic Multidecadal Oscillation since 1567 A.D. *Geophys Res Lett* 31:L12205. doi: [10.1029/2004GL019932](https://doi.org/10.1029/2004GL019932)
- Grosfeld K, Lohmann G, Rimbu N, Fraedrich K, Lunkeit F (2007) Atmospheric multidecadal variations in the North Atlantic realm: proxy data, observations, and atmospheric circulation model studies. *Clim Past* 3. www.clim-past.net/3/39/2007/39-50
- Grosfeld K, Lohmann G, Rimbu N (2008) The impact of Atlantic and Pacific Ocean sea surface temperature anomalies on the North Atlantic multidecadal variability. *Tellus A*. doi: [10.1111/j.1600-0870.2008.00304.x](https://doi.org/10.1111/j.1600-0870.2008.00304.x)
- GYa Vangenheim (1940) The long-term temperature and ice break-up forecasting. *Proc State Hydrol Inst Iss* 10:207–236 (in Russian)
- Hakkinen S (1999) A simulation of thermohaline effects of a great salinity anomaly. *J Clim* 12:1781–1795
- Hansen DV, Bedzek HF (1996) On the nature of decadal anomalies in North Atlantic SST. *JGR* 101:8749–8758
- Hilmer M, Jung T (2000) Evidence for a recent change in the link between the North Atlantic Oscillations and Arctic sea ice export. *Geophys Res Lett* 27(7):989–992. doi: [10.1029/1999GL010944](https://doi.org/10.1029/1999GL010944)
- Hurrell JW (1995) Decadal trends in the North Atlantic Oscillation: regional temperatures and precipitation. *Science* 269:676–679
- Jones PD, Moberg A (2003) Hemispheric and large-scale surface air temperature variations: an extensive revision and an update to 2001. *J Clim* 16:206–223. doi: [10.1175/1520-0442\(2003\)16<206:206-223>2.0.CO;2](https://doi.org/10.1175/1520-0442(2003)16<206:206-223>2.0.CO;2)
- Kaplan A, Cane M, Kushnir Y, Clement A, Blumenthal M, Rajagopalan B (1998) Analyses of global sea surface temperature 1856–1991. *J Geophys Res* 103:18, 567–18, 589
- Keenlyside NS, Latif M, Jungclauss J, Kornbluh L, Roeckner E (2008) Advancing decadal-scale climate prediction in the North Atlantic sector. *Nature* 453:84–88. doi: [10.1038/nature06921](https://doi.org/10.1038/nature06921)
- Kelly K, Dong S (2004) The relationship of western boundary current heat transport and storage to midlatitude ocean–atmosphere interaction. In: Wang C, Xie S-P, Carton JA (eds) Ocean–atmosphere interaction and climate variability. AGU monograph
- Kerr RA (2000) A North Atlantic climate pacemaker for the centuries. *Science* 288:1984–1986. doi: [10.1126/science.288.5473.1984](https://doi.org/10.1126/science.288.5473.1984)
- Kirov B, Georgieva K (2002) Long-term variations and interrelations of ENSO, NAO, and solar activity. *Phys Chem Earth* 27:441–448
- Klyashtorin LB, Lyubushin AA (2007) Cyclic climate changes and fish productivity. VNIRO Publishing, Moscow. Editor for English version: Dr. Gary D. Sharp, Center for Climate/Ocean Resources Study, Salinas
- Knight JR, Allan RJ, Folland CK, Vellinga M, Mann ME (2005) A signature of persistent natural thermohaline circulation cycles in observed climate. *Geophys Res Lett* 32:L20708. doi: [10.1029/2005GRL024233](https://doi.org/10.1029/2005GRL024233)
- Knight JR, Folland CK, Scaife AA (2006) Climate impacts of the Atlantic Multidecadal Oscillation. *Geophys Res Lett* 33:L17706. doi: [10.1029/2006GL026242](https://doi.org/10.1029/2006GL026242)
- Kondrashov D, Ghil M (2006) Spatio-temporal filling of missing points in geophysical data sets. *Nonlin Proc Geophys* 13:151–159

- Kravtsov S (2011) An empirical model of decadal ENSO variability. *J Clim* (submitted)
- Kravtsov S, Kondrashov D, Ghil M (2005) Multi-level regression modeling of nonlinear processes: derivation and applications to climatic variability. *J Clim* 18:4404–4424. doi:[10.1175/JCLI3544.1](https://doi.org/10.1175/JCLI3544.1)
- Kravtsov S, Dewar WK, Ghil M, McWilliams JC, Berloff P (2008) A mechanistic model of mid-latitude decadal climate variability. *Phys D* 237:584–599. doi:[10.1016/j.physd.2007.09.025](https://doi.org/10.1016/j.physd.2007.09.025)
- Kushnir Y (1994) Interdecadal variations in North Atlantic sea surface temperature and associated atmospheric conditions. *J Clim* 7(1):141–157
- Kushnir Y, Held I (1996) Equilibrium atmospheric response to North Atlantic SST anomalies. *J Clim* 9:1208–1220
- Kushnir Y, Robinson WA, Blade I, Hall NMJ, Peng S, Sutton R (2002) Atmospheric GCM response to extratropical SST anomalies: synthesis and evaluation. *J Clim* 15:2233–2256
- Kwon Y, Alexander MA, Bond NA, Frankignoul C, Nakamura H, Qiu B, Thompson L (2010) Role of the Gulf Stream and Kuroshio–Oyashio systems in large-scale atmosphere–ocean interaction: a review. *J Clim Spec Collection*. doi:[10.1175/2010JCLI3343.1](https://doi.org/10.1175/2010JCLI3343.1)
- Latif M, Barnett TP (1994) Causes of decadal climate variability over the North Pacific and North America. *Science* 266:634–637
- Latif M, Barnett TP (1996) Decadal climate variability over the North Pacific and North America: dynamics and predictability. *J Clim* 9:2407–2423
- Latif M, Arpe K, Roeckner E (2000) Oceanic control of decadal North Atlantic sea level pressure variability in winter. *Geophys Res Lett* 27:727–730. doi:[10.1029/1999GL002370](https://doi.org/10.1029/1999GL002370)
- Latif M, Roeckner E, Botzet M, Esch M, Haak H, Hagemann S, Jungclaus J, Legutke S, Marsland S, Mikolajewicz U, Mitchell J (2004) Reconstructing, monitoring, and predicting decadal-scale changes in the North Atlantic thermohaline circulation with sea surface temperature. *J Clim* 17:1605–1614. doi:[10.1175/1520-0442\(2004\)](https://doi.org/10.1175/1520-0442(2004)17<1605:RMACT>2.0.CO;2)
- Latif M, Böning C, Willebrand J, Biastoch A, Dengg J, Keenlyside N, Schweckendiek U, Madec G (2006) Is the thermohaline circulation changing? *J Clim* 19(18):4631–4637. doi:[10.1175/JCLI3876.1](https://doi.org/10.1175/JCLI3876.1)
- Lau N-C, Nath MJ (1994) A modeling study of the relative roles of tropical and extratropical SST anomalies in the variability of the global atmosphere–ocean system. *J Clim* 7:1184–1207
- Mann ME, Park J (1994) Global-scale modes of surface temperature variability on interannual to century timescales. *J Geophys Res* 99:25819–25833
- Mann ME, Park J (1996) Joint spatiotemporal modes of surface temperature and sea level pressure variability in the Northern Hemisphere during the last century. *J Clim* 9:2137–2162
- Mann ME, Park J, Bradley RS (1995) Global interdecadal and century-scale oscillations during the past five centuries. *Nature* 378:266–270
- Mann ME, Bradley RS, Hughes MK (1998) Global-scale temperature patterns and climate forcing over the past six centuries. *Nature* 392:779–787
- Mantua NJ, Hare SR, Zhang Y, Wallace JM, Francis RC (1997) A Pacific interdecadal climate oscillation with impacts on salmon production. *Bull Am Meteorol Soc* 78:1069–1079
- Marshall J, Johnson H, Goodman J (2001a) A study of the interaction of the North Atlantic Oscillation with ocean circulation. *J Clim* 14:1399–1421
- Marshall J, Kushnir Y, Battisti D, Chang P, Czaja A, Dickson R, Hurrell J, McCartney M, Saravanan R, Visbeck M (2001b) North Atlantic climate variability: phenomena, impacts and mechanisms. *Int J Climatol* 21:1863–1898. doi:[10.1002/joc.693](https://doi.org/10.1002/joc.693)
- McCartney M (1997) Climate change: is the ocean at the helm? *Nature* 388:521–522
- Mehta VM, Suarez MJ, Manganello JV, Delworth TL (2000) Oceanic influence on the North Atlantic Oscillation and associated Northern Hemisphere climate variations: 1959–1993. *Geophys Res Lett* 27(1):121–124. doi:[10.1029/1999GL002381](https://doi.org/10.1029/1999GL002381)
- Metzger EJ, Hurlburt HE (2001) The importance of high horizontal resolution and accurate coastline geometry in modeling South China Sea Inflow. *Geophys Res Lett* 28(6):1059–1062. doi:[10.1029/2000GL012396](https://doi.org/10.1029/2000GL012396)
- Minobe S (1997) A 50–70-year climatic oscillation over the North Pacific and North America. *Geophys Res Lett* 24:683–686
- Minobe S (1999) Resonance in bidecadal and pentadecadal climate oscillations over the North Pacific: role in climatic regime shifts. *Geophys Res Lett* 26:855–858
- Minobe S, Kuwano-Yoshida A, Komori N, Xie S-P, Small RJ (2008) Influence of the Gulf Stream on the troposphere. *Nature* 452:206–209. doi:[10.1038/nature06690](https://doi.org/10.1038/nature06690)
- Moron V, Vautard R, Ghil M (1998) Trends, interdecadal and interannual oscillations in global sea-surface temperatures. *Clim Dyn* 14:545–569
- Msadek R, Dixon KW, Delworth TL, Hurlin W (2010a) Assessing the predictability of the Atlantic meridional overturning circulation and associated fingerprints. *Geophys Res Lett* 37:L19608. doi:[10.1029/2010GL044517](https://doi.org/10.1029/2010GL044517)
- Msadek R, Frankignoul C, Li LZ (2010b) Mechanisms of the atmospheric response to North Atlantic multidecadal variability: a model study. *Clim Dyn*. doi:[10.1007/s00382-010-0958-0](https://doi.org/10.1007/s00382-010-0958-0)
- Nakamura H, Sampe T, Tanimoto Y, Shimpō A (2004) Observed associations among storm tracks, jet streams, and midlatitude ocean fronts. from AGU monograph: the earth's climate: the ocean–atmosphere interaction geophysical monograph, vol 147, pp 329–346. doi:[10.1029/147GM18](https://doi.org/10.1029/147GM18)
- North GR, Bell TL, Cahalan RF, Moeng FJ (1982) Sampling errors in the estimation of empirical orthogonal functions. *Mon Wea Rev* 110:669–706
- Overland JE, Adams JM, Bond NA (1999) Decadal variability of the Aleutian low and its relation to high-latitude circulation. *J Clim* 12:1542–1548
- Palmer TN, Sun Z (1985) A modeling and observational study of the relationship between sea surface temperature in the northwest Atlantic and the atmospheric general circulation. *QJR Meteorol Soc* 111:947–975
- Peng S, Robinson WA (2001) Relationships between atmospheric internal variability and the response to an extratropical SST anomaly. *J Clim* 14:2943–2959. doi:[10.1175/1520-0442\(2001\)](https://doi.org/10.1175/1520-0442(2001)14<2943:RIBVA>2.0.CO;2)
- Peng S, Whitaker JS (1999) Mechanisms determining the atmospheric response to midlatitude SST anomalies. *J Clim* 12:1393–1408
- Peng S, Robinson WA, Hoerling MP (1997) The modeled atmospheric response to midlatitude SST anomalies and its dependence on background circulation states. *J Clim* 10:971–987
- Peng S, Robinson WA, Li S (2002) North Atlantic SST forcing of the NAO and relationships with intrinsic hemispheric variability. *Geophys Res Lett* 29:1276. doi:[10.1029/2001GL014043](https://doi.org/10.1029/2001GL014043)
- Penland C (1989) Random forcing and forecasting using principal oscillation pattern analysis. *Mon Wea Rev* 117:2165–2185
- Penland C (1996) A stochastic model of Indo-Pacific sea-surface temperature anomalies. *Phys D* 98:534–558
- Penland C, Ghil M (1993) Forecasting Northern Hemisphere 700-mb geopotential height anomalies using empirical normal modes. *Mon Wea Rev* 121:2355–2372
- Pohlmann H, Sienz F, Latif M (2006) Influence of the multidecadal Atlantic meridional overturning circulation variability on European climate. *J Clim* 19:6062–6067 (special section). doi:[10.1175/JCLI3941.1](https://doi.org/10.1175/JCLI3941.1)
- Polonsky AB, Basharin DV, Voskresenskaya EN, Worley SJ, Yurovsky AV (2004) Relationship between the North Atlantic

- Oscillation, Euro-Asian climate anomalies and Pacific variability. *Mar Meteorol Pac Oceanogr* 2(1–2):52–66
- Polyakov IV, Alexeev VA, Bhatt US, Polyakova EI, Zhang X (2009) North Atlantic warming: patterns of long-term trend and multidecadal variability. *Clim Dyn* (Springerlink.com). doi: [10.1007/s00382-008-0522-3](https://doi.org/10.1007/s00382-008-0522-3)
- Preisendorfer RW (1988) *Principal component analysis in meteorology and oceanography*. Elsevier, Amsterdam
- Press WH, Teukolsky SA, Vetterling WT, Flannery BP (1994) *Numerical recipes*, 2nd edn. Cambridge University Press, Cambridge
- Rayner NA, Brohan P, Parker DE, Folland CK, Kennedy J, Vanicek M, Ansell T, Tett SFB (2006) Improved analyses of changes and uncertainties in sea-surface temperature measured in situ since the mid-nineteenth century. *J Clim* 19:446–469. doi: [10.1175/JCLI3637.1](https://doi.org/10.1175/JCLI3637.1)
- Robertson AW, Mechoso CR, Kim Y-J (2000) The influence of Atlantic sea surface temperature anomalies on the North Atlantic Oscillation. *J Clim* 13:122–138. doi: [10.1175/1520-0442\(2000\)13:122-138](https://doi.org/10.1175/1520-0442(2000)13<122:IOASST>2.0.CO;2)
- Rodwell MJ, Rowell DP, Folland CK (1999) Oceanic forcing of the wintertime North Atlantic Oscillation and European climate. *Nature* 398:320–323
- Rogers JC (1981) The North Pacific Oscillation. *Int J Climatol* 1:39–57
- Schlesinger ME, Ramankutty N (1994) An oscillation in the global climate system of period 65–70 years. *Nature* 367:723–726
- Schneider T (2001) Analysis of incomplete climate data: estimation of mean values and covariance matrices and imputation of missing values. *J Clim* 14:853–871. doi: [10.1175/1520-0442\(2001\)14:853-871](https://doi.org/10.1175/1520-0442(2001)14<853:AIICLD>2.0.CO;2)
- Shabalova MV, Weber SL (1999) Patterns of temperature variability on multidecadal to centennial timescales. *J Geophys Res* 104:31023–31041
- Shaffrey L, Sutton R (2006) Bjerknes compensation and the decadal variability of the energy transports in a coupled climate model. *J Clim* 19:1167–1181. doi: [10.1175/JCLI3652.1](https://doi.org/10.1175/JCLI3652.1)
- Shindell DT, Schmidt GA, Miller RL, Rind D (2001) Northern Hemisphere winter climate response to greenhouse gas, ozone, solar, and volcanic forcing. *J Geophys Res* 106:7193–7210. doi: [10.1029/2000JD900547](https://doi.org/10.1029/2000JD900547)
- Stocker TF, Mysak LA (1992) Climatic fluctuations on the century time scale: a review of high-resolution proxy data and possible mechanisms. *Clim Change* 20:227–250
- Sugimoto S, Hanawa K (2009) Decadal and interdecadal variations of the aleutian low activity and their relation to upper oceanic variations over the North Pacific. *J Meteorol Soc Jpn* 87(4):601–614. doi: [10.2151/jmsj.87.601](https://doi.org/10.2151/jmsj.87.601)
- Sutton RT, Allen MR (1997) Decadal predictability of North Atlantic sea surface temperature and climate. *Nature* 388:563–567
- Sutton RT, Hodson DLR (2003) Influence of the ocean on North Atlantic climate variability 1871–1999. *J Clim* 16:3296–3313. doi: [10.1175/1520-0442\(2003\)16:3296-3313](https://doi.org/10.1175/1520-0442(2003)16<3296:IOASST>2.0.CO;2)
- Sutton RT, Hodson DLR (2005) Atlantic Ocean forcing of North American and European summer climate. *Science* 309:115–118. doi: [10.1126/science.1109496](https://doi.org/10.1126/science.1109496)
- Sutton RT, Hodson DLR (2007) Climate response to basin-scale warming and cooling of the North Atlantic Ocean. *J Clim* 20:891–907. doi: [10.1175/JCLI4038.1](https://doi.org/10.1175/JCLI4038.1)
- Sutton RT, Hodson DLR, Mathieu P (2003) The role of the Atlantic Ocean in climate forecasting. *Proceedings of the ECMWF workshop on the role of the upper ocean in medium and extended range forecasting*, ECMWF, Reading
- Swanson K, Tsonis AA (2009) Has the climate recently shifted? *Geophys Res Lett* 36. doi: [10.1029/2008GL037022](https://doi.org/10.1029/2008GL037022)
- Timmermann A, Latif M, Voss R, Grotzner A (1998) Northern Hemispheric interdecadal variability: a coupled air-sea mode. *J Clim* 11:1906–1931
- Timmermann A, Okumura Y, An SI, Clement A, Dong B, Guilyardi E, Hu A, Jungclaus JH, Renold M, Stocker TF, Stouffer RJ, Sutton R, Xie SP, Yin J (2007) The influence of a weakening of Atlantic meridional overturning circulation on ENSO. *J Clim* 20:4899–4919. doi: [10.1175/JCLI4283.1](https://doi.org/10.1175/JCLI4283.1)
- Tsonis AA, Swanson K, Kravtsov S (2007) A new dynamical mechanism for major climate shifts. *Geophys Res Lett* 34:L13705. doi: [10.1029/2007GL030288](https://doi.org/10.1029/2007GL030288)
- Van der Swaluw E, Drijfhout SS, Hazeleger W (2007) Bjerknes compensation at high northern latitudes: the ocean forcing the atmosphere. *J Clim* 20:6023–6032. doi: [10.1175/2007JCLI1562.1](https://doi.org/10.1175/2007JCLI1562.1)
- Vautard R, Ghil M (1989) Singular spectrum analysis in nonlinear dynamics, with applications to paleoclimatic time series. *Phys D* 35:395–424
- Vautard R, Yiou P, Ghil M (1992) Singular spectrum analysis: a toolkit for short, noisy and chaotic series. *Phys D* 58:95–126
- Vellinga M, Wood RA (2002) Global climatic impacts of a collapse of the Atlantic thermohaline circulation. *Clim Change* 54:251–267. doi: [10.1023/A:1016168827653](https://doi.org/10.1023/A:1016168827653)
- Vellinga M, Wu P (2004) Low-latitude freshwater influence on centennial variability of the Atlantic thermohaline circulation. *J Clim* 17:4498–4511. doi: [10.1175/3219.1](https://doi.org/10.1175/3219.1)
- Vimont DJ, Kossin JP (2007) The Atlantic meridional mode and hurricane activity. *Geophys Res Lett* 34:L07709. doi: [10.1029/2007GL029683](https://doi.org/10.1029/2007GL029683)
- Vimont DJ, Battisti DS, Hirst AC (2001) Footprinting: a seasonal connection between the tropics and mid-latitudes. *Geophys Res Lett* 28:3923–3926
- Vimont DJ, Battisti DS, Hirst AC (2003a) The seasonal footprinting mechanism in the CSIRO general circulation models. *J Clim* 16:2653–2667. doi: [10.1175/1520-0442\(2003\)16:2653-2667](https://doi.org/10.1175/1520-0442(2003)16<2653:SFME>2.0.CO;2)
- Vimont DJ, Wallace JM, Battisti DS (2003b) The seasonal footprinting mechanism in the Pacific: implications for ENSO. *J Clim* 16:2668–2675
- Walker GT, Bliss EW (1932) *World weather*. Mem R Meteorol Soc 4:53–84
- Wallace JM, Gutzler DS (1981) Teleconnections in the geopotential height field during the Northern Hemisphere winter. *Mon Wea Rev* 109:784–812
- Wang L, Chen W, Huang R (2007) Changes in the variability of North Pacific oscillation around 1975/1976 and its relationship with East Asian winter climate. *J Geophys Res* 112:D11110. doi: [10.1029/2006JD008054](https://doi.org/10.1029/2006JD008054)
- Willis JK, Roemmich D, Cornuelle B (2004) Interannual variability in upper ocean heat content, temperature, and thermosteric expansion on global scales. *J Geophys Res* 109:C12036. doi: [10.1029/2003C002260](https://doi.org/10.1029/2003C002260)
- Wu P, Gordon C (2002) Oceanic influence on North Atlantic climate variability. *J Clim* 15:1911–1925. doi: [10.1175/1520-0442\(2002\)15:1911-1925](https://doi.org/10.1175/1520-0442(2002)15<1911:OIOASST>2.0.CO;2)
- Wu LP, Rodwell M (2004) Gulf Stream forcing of the winter North Atlantic Oscillation. *Atmos Sci Lett* 5:57–64. doi: [10.1016/j.atmoscilet.2003.12.002](https://doi.org/10.1016/j.atmoscilet.2003.12.002)
- Xie SP (2004) Satellite observations of cool ocean-atmosphere interaction. *Bull Am Meteorol Soc* 85:195–208. doi: [10.1175/BAMS-85-2-195](https://doi.org/10.1175/BAMS-85-2-195)
- Xie SP, Carton J (2004) Tropical Atlantic variability: patterns, mechanisms, and impacts. *Earth climate: the ocean-atmosphere interaction*. In: Wang C, Xie SP, Carton JA (eds) *Geophys monograph*. AGU, Washington, DC, pp 121–142. doi: [10.1029/147GM07](https://doi.org/10.1029/147GM07)
- Yualeva EN, Schneider N, Pierce DW, Barnett TP (2001) Modeling of North Pacific climate variability forced by ocean heat flux anomalies. *J Clim* 14:4027–4046. doi: [10.1175/1520-0442\(2001\)14:4027-4046](https://doi.org/10.1175/1520-0442(2001)14<4027:NPCLV>2.0.CO;2)
- Zhang R, Delworth TL (2005) Simulated tropical response to a substantial weakening of the Atlantic thermohaline circulation. *J Clim* 18:1853–1860. doi: [10.1175/JCLI3460.1](https://doi.org/10.1175/JCLI3460.1)

- Zhang R, Delworth TL (2007) Impact of Atlantic multidecadal oscillations on India/Sahel rainfall and Atlantic hurricanes. *Geophys Res Lett* 33:L17712. doi:[10.1029/2006GL026267](https://doi.org/10.1029/2006GL026267)
- Zhang YJ, Wallace M, Iwasaka N (1996) Is climate variability over the North Pacific a linear response to ENSO? *J Clim* 9:1468–1478
- Zhang R, Delworth TL, Held IM (2007) Can the Atlantic Ocean drive the observed multidecadal variability in Northern Hemisphere mean temperature? *Geophys Res Lett* 34:L02709. doi:[10.1029/2006GL028683](https://doi.org/10.1029/2006GL028683)
- Zhen-Shan L, Xian S (2007) Multi-scale analysis of global temperature changes and trend of a drop in temperature in the next 20 years. *Meteorol Atmos Phys* 95:115–121